

AperTO - Archivio Istituzionale Open Access dell'Università di Torino

Late-Alpine rodingitization in the Bellecombe meta-ophiolites (Aosta Valley, Italian Western Alps): evidence from mineral assemblages and serpentinization-derived H₂-bearing brine.

This is the author's manuscript

Original Citation:

Availability:

This version is available <http://hdl.handle.net/2318/79610> since

Published version:

DOI:10.1080/00206810903557761

Terms of use:

Open Access

Anyone can freely access the full text of works made available as "Open Access". Works made available under a Creative Commons license can be used according to the terms and conditions of said license. Use of all other works requires consent of the right holder (author or publisher) if not exempted from copyright protection by the applicable law.

(Article begins on next page)



UNIVERSITÀ DEGLI STUDI DI TORINO

This is an author version of the contribution published on:

Questa è la versione dell'autore dell'opera:

International Geology Review, 52, 2010, doi: 10.1080/00206810903557761

The definitive version is available at:

La versione definitiva è disponibile alla URL:

<http://www.tandfonline.com/toc/tigr20/52/10-12#.UwN8KM4f6q0>

1 **Late-Alpine Rodingitisation in the Bellecombe Meta-ophiolites (Aosta Valley, Italian**
2 **Western Alps): Evidence from Mineral Assemblages**
3 **and Serpentinization-derived H₂-bearing Brine**
4

5 SIMONA FERRANDO¹, MARIA LUCE FREZZOTTI², PAOLO ORIONE¹, RICCARDO CARLO CONTE¹,
6 ROBERTO COMPAGNONI¹
7

8 ¹ Department of Mineralogical and Petrological Sciences, University of Torino, Via Valperga
9 Caluso 35, I-10125 Torino, Italy

10 ² Department of Earth Sciences, University of Siena, Via Laterina 8, I-53100 Siena, Italy
11

12
13
14 Corresponding author:

15 Dr. Simona Ferrando

16 E-mail address: simona.ferrando@unito.it
17

18 Submitted to:

19 International Geology Review, Special Issue: *Alpine Concepts in Geology*

20 **Revised Ms**
21

22 **Abstract**
23

24 We report on Alpine metamorphic and fluid inclusion evolution of a poly-phase rodingite
25 occurrence within the Bellecombe antigorite-serpentinite, exposed in the Piemonte Zone of
26 Aosta Valley, NW Italy. Fine-grained rodingitic rocks, derived from a protolith of basaltic dyke(s),
27 are cross-cut by a network of at least six vein generations, consisting of chlorite, diopside, and
28 grossular garnet (Type I), andradite-grossular garnet + diopside (Type II), andradite-rich garnet
29 + chlorite (Type III), grossular-rich garnet (Type IV), vesuvianite (Type V), and chlorite (Type VI).
30 The fine-grained rodingite and associated veins reveal a tectono-metamorphic history similar to
31 that of the hosting serpentinite and characterised by an earlier HP metamorphism, followed by
32 decompression/re-equilibration under greenschist-facies conditions and by final cooling. The
33 fluid inclusion study, performed on primary fluid inclusions in vesuvianite from Type V veins and

1 on secondary fluid inclusions in andradite-rich garnet from Type III veins, revealed that at $P =$
2 0.22 GPa and $T = 400^\circ\text{C}$ a H_2 -bearing ($X_{\text{H}_2}=0.010$) brine (6 wt % CaCl_2 + 6 wt % NaCl) with
3 traces of CH_4 ($X_{\text{CH}_4}=0.002$) was introduced into the rock. This fluid had a composition
4 compatible with the Ca-rich H_2 -bearing, reducing aqueous solutions reported from the
5 serpentinization front. These data point to an important event of rodingitisation during the late
6 greenschist-facies Alpine evolution that was probably triggered by hydration of metamorphic
7 olivine.

8

9 *Key-words:* metasomatism, rodingite, serpentinite, veins, vesuvianite, fluid inclusions, hydrogen,
10 methane.

11

12 **Introduction**

13

14 Rodingites are calcium-rich, silica undersaturated rocks consisting of Ca and Ca-Mg silicates
15 formed by metasomatism of mostly mafic rocks (see e.g. Fettes & Desmons, 2007). At different
16 degrees of metasomatism, rodingites with contrasting mineral assemblages are produced
17 (Schandl et al., 1989), ranging from epidote-rich (epidote *s.l.* including minor diopside and
18 titanite), through grossular-rich (hydrogrossular, prehnite and minor diopside), to diopside-rich
19 compositions. Rodingites included in, or adjacent to, serpentinites occur in ophiolitic complexes
20 from Archaean (e.g. Schandl et al., 1989) to Recent (Honnorez and Kirst, 1975) terranes. On
21 the basis of its occurrence and geochemistry (Palandri and Reed, 2004), rodingitisation is
22 considered to be genetically related to serpentinisation (see e.g. Thayer, 1966; Coleman, 1977).
23 In particular, the aqueous fluids percolating during serpentinisation are supposed to carry Ca
24 and Si released from the break-down of clinopyroxene (e.g.: Iyer et al., 2008), and H_2 released
25 during magnetite production. Ca-oversaturation of this fluid produces metasomatism

1 (rodingitisation) in the mafic rocks (Frost and Beard, 2007 and references therein). Typically, a
2 first episode of rodingitisation occurs during ocean-floor metamorphism; however, ophiolite
3 complexes that are incorporated in orogenic belts may undergo at least another important
4 episode of serpentinitisation and rodingitisation (Dal Piaz et al., 1980; Wares and Martin, 1980;
5 Rösli et al., 1991; Mittwede and Schandl, 1992; O'Hanley et al., 1992; Castelli et al., 1995; Li et
6 al., 2007; Normand and Williams-Jones, 2007).

7

8 Direct evidence of the composition of the fluids responsible for rodingitisation comes from fluid
9 inclusion studies. Schandl et al. (1990) reported on the composition of the fluid phase present
10 during ocean-floor rodingitisation of the Achaean Abitibi greenstone belt (Bowman mine): it is a
11 very-low salinity (1.6 wt % NaCl_{eq}) aqueous fluid ($X_{\text{H}_2\text{O}}=0.988$) with minor CH₄ ($X_{\text{CH}_4}=0.004$),
12 C₃H₆ ($X_{\text{C}_3\text{H}_6} = 0.001$), C₃H₈ ($X_{\text{C}_3\text{H}_8} = 0.007$), and traces of N₂ (96 ppm). In metamorphic
13 environments, various fluid inclusion studies have revealed the presence of relatively saline ($8 \pm$
14 1.5 wt % NaCl_{eq}) brines in rodingites [e.g. British Columbia, O'Hainley et al. (1992); southern
15 Appalachian Piedmont: Mittwede and Schandl (1992); Lanzo Massif, Alps: Castelli et al., 1995],
16 generally trapped at different stages during the retrograde metamorphic evolution.

17

18 In spite of ample geochemical evidence for the presence of reduced fluids in ophiolite
19 complexes, H₂ has been very rarely detected in fluid inclusions from metamorphic
20 environments. In the Malenco peridotite, Peretti et al. (1992) described the presence of H₂ (0.3 –
21 3 mol%) within brines (5.1 wt % CaCl₂ + 6.4 wt % NaCl), that they postulated to have formed by
22 de-serpentinitisation during prograde Alpine metamorphism. Gas chromatographic analyses on
23 rodingites from the Karabash massif (southern Urals) revealed that the fluid responsible for
24 rodingitisation is an aqueous fluid (2.6 – 8.0 wt% NaCl_{eq}) containing H₂, minor CO₂ and CH₄,
25 and traces of CO and N₂ (Murzin and Shanina, 2007). Also the serpentinitisation-fluid analyzed in

1 serpentinites hosting rodingites is water dominated, but is characterised by higher CO₂, and only
2 minor H₂, CO, and CH₄ contents (Murzin and Shanina, 2007). Gas chromatographic analyses
3 on rodingites from the JM Asbestos mine (Québec; Canada) showed that the fluid responsible
4 for rodingitisation is aqueous, containing CH₄, C₂H₆, *n*-C₄H₁₀, *n*-C₅H₁₂ and minor amounts of N₂
5 or CO, Ar, and H₂ (Normand and William-Jones, 2007).

6
7 In this study, we present petrological and fluid inclusion data for a rodingitisation event, which
8 occurred in an already-rodingitised dyke hosted in a Bellecombe antigorite-serpentinite (Aosta
9 Valley, Italian Western Alps). This secondary rodingitisation was caused by serpentinisation-
10 derived H₂-bearing brines pervasively infiltrating the pre-existing rodingite during late stages of
11 the Alpine orogenic history.

12 13 **Previous studies and geological setting**

14
15 In the Alps, rodingitised metagabbroid and metabasaltic dykes have been extensively reported
16 from the Piemonte ophiolite nappes (e.g.: Dal Piaz, 1967; Bezzi and Piccardo, 1969; Evans et
17 al., 1979; Piccardo et al., 1980; Dietrich et al., 1986; Rösly, 1988; Castelli et al., 1995; Ferraris
18 and Compagnoni, 2003). The studied rodingites from the Bellecombe area are hosted in
19 serpentinites belonging to the metaophiolites of the Zermatt-Saas Unit of the Piemonte Zone,
20 Western Alps (Fig. 1). The Zermatt-Saas Unit consists of metamorphic ophiolites and related
21 metasedimentary rocks (calcschists or “schistes lustrés”) derived from the floor of the Mesozoic
22 Piemonte-Liguria ocean (e.g. Dal Piaz et al., 1980). After the ocean-floor metamorphism, the
23 Zermatt-Saas metaophiolites experienced the Alpine orogeny, recording an early eclogite-facies
24 and a later greenschist-facies metamorphic overprint (see e.g., Borghi et al., 1996; Castelli et
25 al., 1995; Li et al., 2004a).

1

2 In the Zermatt-Saas Unit, Dal Piaz and Grasso (1967) reported the presence of rodingites from
3 the serpentinites intersected by the “Petit Monde” tunnel of the Torino-Aosta motor-way (Fig. 1).

4 The rodingites consist of ugranditic garnet, chlorite, diopside, vesuvianite, clinozoisite and a
5 relict magmatic clinopyroxene. In the nearby, upper Valtournenche-Breuil area, Aosta Valley,

6 Dal Piaz et al. (1980) reported relict HP minerals, such as Na-rich pyroxene, from the less
7 rodingitised boudins from Les Perères-Gouffre de Bousserailles, Gobba di Rollin, and Goillet

8 (Fig. 1). More recently, Li et al. (2004a, b, 2008) described the Zermatt-Saas rodingites and the

9 hosting serpentinites from the Lichenbretter area, Swiss Western Alps (Fig. 1). Although all

10 rodingites contain vesuvianite, chlorite and hydrogrossular, three different types were

11 distinguished on the basis of additional minerals. The first type contains diopside, tremolite,

12 clinozoisite and calcite; the second type hydroandradite, diopside, epidote and calcite; the third

13 type only hydroandradite. These three different rodingite types were interpreted as

14 representative of different protoliths, characterised by different Fe^{3+}/Fe^{2+} ratios acquired during

15 an early ocean-floor rodingitisation ($T \cong 200 \text{ }^{\circ}\text{C}$; $P \cong 0.2 \text{ GPa}$). Subsequently, these rocks

16 underwent the Alpine orogenic cycle, including an early HP stage ($T = 600^{\circ}\text{C}$; $P = 2.5\text{-}3.0 \text{ GPa}$),

17 a second post-nappe emplacement greenschist-facies metamorphic stage ($T = 400\text{-}450^{\circ}\text{C}$; $P =$

18 $0.3\text{-}0.5 \text{ GPa}$), and a late sub-greenschist-facies stage ($T \cong 300^{\circ}\text{C}$; $P \cong 0.2 \text{ GPa}$). During the HP

19 peak, the rodingites experienced a second rodingitisation event triggered by the fluid released

20 from dehydration of the nearby serpentinites (Li et al., 2008).

21

22 In recent papers, Panseri et al. (2008) and Fontana et al. (2008) described “rodingitic dykes”

23 (i.e., basaltic or gabbroid dykes transformed into rodingites) and the hosting serpentinites from

24 the southern side of the Mount Avic (Southern Aosta Valley, Fig. 1). Different types of rodingites

25 were distinguished on the basis of the mineral assemblages: 1) “garnet-rodingitic dyke” (garnet

1 + chlorite ± diopside ± vesuvianite); 2) “vesuvianite-rodingitic dyke” (vesuvianite + chlorite ±
2 garnet); 3) “foliated rodingite” (diopside + chlorite); 4) “rodingitic reaction zones” at the contact
3 between metabasite and serpentinite (garnet + epidote + chlorite). To explain these different
4 types of rodingites, the authors suggested possible differences in the chemistry of the protolith,
5 consequent to different extents of either the oceanic rodingitisation or the Alpine metamorphic
6 overprint.

7

8 **Analytical methods**

9

10 Mineral analyses were obtained with a *Cambridge Instruments* SEM-EDS at the Department of
11 Mineralogical and Petrological Sciences, the University of Torino. Operating conditions were 15
12 kV accelerating voltage and 50 s counting time. Natural and synthetic mineral and oxide
13 standards were employed. Structural formulae were processed using the NORM software of
14 Ulmer (1986). For pyroxenes the $\text{Fe}^{3+}/\text{Fe}^{2+}$ ratio was calculated following the method of Lindsley
15 and Anderson (1983). For chlorites all Fe has been considered as Fe^{2+} . Mineral abbreviations
16 are after Kretz (1983).

17 The micro-Raman spectra of minerals were obtained at the Department of Mineralogical and
18 Petrological Sciences, the University of Torino with an integrated micro/macro-Raman LABRAM
19 HRVIS (Horiba Jobin Yvon Instruments) characterised by an excitation line at 532.11 produced
20 by solid-state Nd laser at 80 mW of emission power, a Super Notch Plus filter with spectral
21 resolution of 1 cm^{-1} , and a grating of 600 grooves/mm. The laser spot size was focussed to 5
22 μm with a 50x objective. Two accumulations in the time span of 15 – 30 s were collected for
23 each *spectrum*. Calibration was performed using the 520.6 cm^{-1} Si band.

24

1 Microthermometry on fluid inclusions was performed using a Chaixmeca heating-freezing stage
2 coupled with a Leitz polarizing microscope (50x objective) at the Department of Mineralogical
3 and Petrological Sciences, the University of Torino. The accuracy, estimated using synthetic
4 fluid inclusion standards, is about 0.2 °C at the triple point of CO₂. Freezing temperature (T_f),
5 eutectic temperature (T_e), final melting temperature of hydrohalite (T_{m_{Hhl}}) and ice (T_{m_{ice}}), and
6 homogenisation temperature to the liquid phase (ThL) were measured. Fluid inclusion
7 compositions, densities, and isochores were determined using the software package FLUID
8 (Bakker, 2003; Bakker and Brown, 2003).

9
10 Micro-Raman analyses on fluid inclusions were collected at the Department of Earth Sciences,
11 the University of Siena, with a confocal Labram multichannel spectrometer (Jobin Yvon
12 Instruments) characterised by an excitation line at 514.5 nm produced by an Ar⁺-ion laser at 500
13 mW of incident power, a Notch holographic filter with a spectral resolution of 1.5 cm⁻¹, and a
14 grating of 1800 grooves/mm. The same double-polished sections used for microthermometric
15 measurements were analysed. The laser spot size was focussed to 1-2 μm with a 100x
16 objective. Accumulation times were 60 s. Calibration was performed using the 1332 cm⁻¹
17 diamond band.

18

19 **Field relationships, petrography and mineral chemistry**

20

21 The Bellecombe rodingites—well known among mineral collectors and museums for their gem-
22 quality minerals—are exposed East of the village near the top of Mont-Avi (Figs. 1 and 2), a
23 small hill corresponding to the top of a deep-seated landslide (Giardino, 1996). Fine-grained and
24 coarse-grained rodingites occur as boudins in sheared antigorite serpentinites, that belong to
25 the Zermatt-Saas zone (Fig. 2) and show a pervasive regional foliation (S_r) deformed by a cm-

1 spaced crenulation cleavage (S_{r+1}). The fine-grained rodingite is boudinaged and the single
2 boudins, 20-50 cm thick, are aligned along and wrapped around by S_r (Fig. 2). They consist of
3 garnet, chlorite, clinopyroxene and vesuvianite and are usually cut by different generations of
4 coarser-grained discontinuous lens-like dilation veins (mm- to cm-thick) with sharp boundaries.
5 Because these metamorphic veins only consist of typical rodingitic minerals, in the following
6 they will be referred to as “rodingitic veins”. A single boudin of a coarse-grained rodingite, most
7 likely deriving from a gabbro protolith, has been also found: it consists of coarse-grained
8 clinopyroxene and chlorite, and fine-grained garnet partly replaced by vesuvianite. The
9 rodingite-serpentinite contacts are systematically marked by 10-30 cm-thick chloritite layers,
10 whose foliation is consistent with that of the hosting serpentinite.

11

12 The examination of 17 samples of the hosting serpentinite and 25 samples of the fine-grained
13 rodingites and associated veins has been performed in this study.

14

15 *The hosting antigorite serpentinite*

16

17 The antigorite serpentinite mainly consists of the following metamorphic minerals: antigorite,
18 diopside, olivine ($Fe_{0.86.0-91.0}Fa_{0.9-1.4}$), titanian-clinohumite ($FeO < 10 \text{ wt\%}$; $Ti O_2 = 6 \text{ wt\%}$), and
19 magnetite, mostly after primary Cr-spinel (Cr_2O_3 up to 28 wt%). The regional foliation (S_r) is
20 defined by the preferred orientation of antigorite, diopside, chlorite and magnetite. The local
21 occurrence of isoclinally folded mm-thick layers mainly consisting of fine-grained olivine,
22 diopside, titanian-clinohumite, antigorite, chlorite and magnetite, with rare porphyroclasts of
23 olivine and titanian-clinohumite, are relics of an older foliation (S_{r-1}). In these layers, earlier
24 deformed metamorphic veins (Type A veins) up to dm-thick, mainly consisting of coarse-grained
25 forsterite + titanian-clinohumite + chlorite, are also present. A younger network of cm- to dm-

1 thick diopside veins (Type B veins) cuts across both type A veins and the S_{r-1} foliation and is
2 deformed by S_r . Recrystallisation of antigorite and chlorite during the development of the
3 crenulation cleavage S_{r+1} is usually observed. Late monomineralic veins (Type C veins),
4 consisting of talc, tremolite, or chrysotile, locally cut across the S_{r+1} . The relics of the peridotitic
5 minerals are: a chromitic spinel partly replaced by a Cr-bearing chlorite [Si > 6.2 atoms per
6 formula unit (a.p.f.u.), $Fe_{tot}/(Fe_{tot}+Mg) < 0.2$; $Fe_{tot} < 2.4$ a.p.f.u.; $Cr_2O_3 > 3$ wt%], a coarse-
7 grained clinopyroxene showing segregation of Cr-rich spinel, and a coarse-grained “bastite”
8 after former peridotitic orthopyroxene. In the more retrogressed samples, metamorphic olivine
9 and diopside are partly to entirely replaced by antigorite and magnetite.

10

11 *The fine-grained rodingite*

12

13 The fine-grained rodingite systematically consists of garnet, chlorite, clinopyroxene, and
14 vesuvianite. Garnet and vesuvianite are locally porphyroblastic. Accessory titanite and a Cr-rich
15 opaque ore are also present. The regional foliation S_r , defined by chlorite, diopside \pm fine-
16 grained garnet, is less evident than in the host serpentinite and is deformed by a cm-spaced
17 crenulation cleavage (S_{r+1} ; Fig. 3a). In spite of this polyphase deformation, microstructural and
18 mineralogical relics of the igneous mafic protolith (see below) are locally preserved (Fig. 3b).

19

20 **Garnet** occurs as both zoned porphyroclasts with a grossular core and an andradite-grossular
21 rim wrapped around by S_r (Fig. 3c), and smaller grossular-andradite neoblasts. The grossular
22 core of porphyroclasts ($Alm_{1-3}Grs_{94-95}Adr_{1-5}$; Fig. 4 and Table 1) includes chlorite, diopside, and
23 titanite after magmatic ilmenite and/or ilmeno-magnetite, whereas the andradite-grossular rim
24 ($Alm_{0-4}Prp_{0-1}Grs_{75-87}Sps_{0-1}Adr_{0-18}Uvr_{0-7}Al-TiGrt_{4-11}$; Fig. 4 and Table 1) is inclusion-free. In the
25 less deformed samples, aggregates of andradite-grossular garnet, grown after former magmatic

1 plagioclase, and interstitial diopside mimic a subophitic microstructure (Fig. 3b). The fine-
2 grained grossular-andradite neoblasts ($\text{Alm}_{0-7} \text{Prp}_{0-2} \text{Grs}_{40-50} \text{Sps}_{0-2} \text{Adr}_{24-54} \text{Uvr}_{0-22} \text{Al-TiGrt}_{1-10}$; Fig.
3 4 and Table 1) occur in samples strongly deformed by S_r (Fig. 3d). A green garnet, with up to 22
4 mole % of uvarovite component, is locally observed around relict Cr-rich spinels, with the Cr-
5 content rapidly decreasing away from the spinel (Fig. 3e). The lack of hydrogarnets is consistent
6 with minerochemical and micro-Raman analyses.

7

8 **Chlorite** occurs in three different microstructural sites: i) as small inclusions within the core of
9 porphyroclastic garnet, ii) as fine-grained lepidoblasts, which define the S_r foliation, and iii) as
10 small crystals surrounding vesuvianite and garnet. In the most pervasively deformed samples, it
11 is evident that chlorite recrystallised later than the development of S_{r+1} . All chlorites have a low
12 Fe-content and plot in the Hey's (1954) field of clinochlore ($\text{Si} = 5.6 - 6.2$ a.p.f.u.; $\text{Fe}^{2+}/(\text{Fe}^{2+} +$
13 $\text{Mg}) = 0 - 0.2$; Table 2).

14

15 **Clinopyroxene** is a diopside, which commonly occurs as poikiloblasts with chlorite inclusions.
16 Thin ilmenite lamellae ($\text{Ilm}_{0.9} \text{Geik}_{0.05} \text{Mn-Ilm}_{0.03}, \text{Hem}_{0.02}$) are present in the core of some
17 crystals (Fig. 3d), and have been interpreted as segregations from a former magmatic Ti-
18 bearing clinopyroxene.

19

20 **Vesuvianite** generally grows at the expense of garnet, commonly preserved as a relict, and is
21 locally zoned with Al increasing and (Ti + Mg) decreasing from core to rim, respectively (Table
22 2). Relics of a **Cr-rich spinel** ($\text{Cr}_2\text{O}_3 = 40 - 55$ wt%, $(\text{FeO} + \text{Fe}_2\text{O}_3) = 35 - 40$ wt%, $\text{MgO} \cong 1$ wt%,
23 and $\text{Al}_2\text{O}_3 > 4$ wt%), partly replaced by magnetite, are surrounded by uvarovitic garnet
24 aggregates (Fig. 3e).

25

1 *The rodingitic veins*

2

3 Six generations of veins, characterised by different mineral assemblage and/or mineral
4 composition and different degree of deformation with respect to the S_r , have been recognised
5 (Table 3). In particular, type I to type III veins are deformed by S_r , whereas type IV to type VI cut
6 across S_r .

7

8 The compositional variations of the different garnet generations in both fine-grained rodingite
9 and rodingitic veins have also been checked by complementary micro-Raman spectroscopy,
10 based on the shifts of the characteristic peaks of grossular (550 cm^{-1} , 832 cm^{-1} , 895 cm^{-1}) which
11 progressively decrease with the increase in the andradite component.

12

13 **Type I veins** are mm-thick, monomineralic and consist of chlorite, granoblastic clinopyroxene,
14 or colourless granoblastic garnet (Table 3). They are deformed by folds, whose axial plane is S_r
15 (Fig. 6a). Locally, type I veins appear to be deformed by the crenulation cleavage. The
16 compositions of both chlorite (clinocllore) and clinopyroxene (diopside) (Table 2) are similar to
17 those of the same minerals in the hosting fine-grained rodingite. Likewise, the composition of
18 the colourless granoblastic garnet ($\text{Alm}_{0-3}\text{GrS}_{93-94}\text{Adr}_{3-6}\text{Al-TiGr}_{0-1}$; Fig. 4 and Table 1) is similar
19 to the grossular core of porphyroclastic garnet of the hosting fine-grained rodingite.

20

21 The **type II veins** are coarse-grained, cut across type I veins, and are always folded by the
22 deformation responsible for the development of S_r . They consist of diopside and a light-pink
23 garnet (Fig. 6b and Table 3), present as crystals elongated perpendicularly to the vein selvages
24 (Fig. 6c). Andradite-grossular garnet ($\text{Alm}_{3-9}\text{Prp}_{1-3}\text{GrS}_{60-68}\text{Sps}_{0-3}\text{Adr}_{13-28}\text{Uvr}_{0-2}\text{AlTiGr}_{2-13}$; Fig. 4
25 and Table 1) is similar to the rim composition of porphyroclastic garnet of the hosting rodingite.

1 Locally, apatite is also present as inclusion in garnet. In some samples, a late growth of
2 vesuvianite after garnet is also observed.

3

4 The **type III veins** (Table 3) consist of a dark-pink andradite-rich garnet ($\text{Alm}_{0.4}\text{Prp}_{0.2}\text{Grs}_{22-}$
5 $_{31}\text{Sps}_{0.1}\text{Adr}_{53-69}\text{Uvr}_{0.3}\text{AlTiGrt}_{1-12}$; Fig. 4 and Table 1) and chlorite (clinocllore). These veins are
6 medium- to coarse-grained and cut across type II veins (Figs. 6b and 6d). A fine-grained corona
7 of grossular-andradite garnet ($\text{Alm}_{0.4}\text{Prp}_{0.2}\text{Grs}_{34-45}\text{Sps}_{0.2}\text{Adr}_{45-65}\text{Uvr}_{0.3}\text{Al-TiGrt}_{0-13}$; Fig. 4 and
8 Table 1), compositionally similar to that defining the S_r foliation in the hosting rodingite, mantles
9 the coarser-grained crystals (Fig. 6e). Locally, these veins are deformed by the crenulation
10 cleavage and the garnet is partly replaced by vesuvianite.

11

12 The rare **type IV veins**, up to 1 mm thick, are monomineralic and cut across type III veins (Fig.
13 6f). They consist of fine-grained garnets richer in the grossular component ($\text{Alm}_{1.9}\text{Prp}_{1.3}\text{Grs}_{50-57}$
14 $\text{Sps}_{0.1}\text{Adr}_{29-37}\text{Uvr}_{0.2}\text{Al-TiGrt}_{2-9}$; Fig. 4 and Table 1) with respect to garnet from type III veins
15 (Table 3). Locally, titanite occurs in the central part of the vein.

16

17 **Type V veins**, which cut across the previous vein generations (Fig. 6g), mainly consist of gem-
18 quality coarse-grained light-pink Al-rich vesuvianite (Table 2 and 3). The wavy extinction shown
19 by vesuvianite suggests its growth before deformation, responsible for the development of the
20 S_{r+1} crenulation.

21

22 **Type VI veins** (Table 3; Fig. 6h) cut across both the previous vein types and S_{r+1} crenulation,
23 and consist of a Fe-rich chlorite (pynochlorite; $\text{Si} = 5.6 - 6.2$ a.p.f.u.; $\text{Fe}^{2+}/(\text{Fe}^{2+} + \text{Mg}) = 0.2 -$
24 0.5 ; Table 2).

25

1 **Fluid inclusion study**

2
3 This study, performed on 18 double-polished 100 μm thick sections of rodingites, have revealed
4 that fluid inclusions occur in two different microstructural sites: i) in the coarse-grained
5 andradite-rich garnet from type III veins, ii) and in the gem-quality vesuvianite from type V veins.
6 The fluid inclusions from type III veins are secondary since they occur as intragranular trails
7 from a grain boundary to another of the host mineral (Fig. 7a; van der Kerkhof and Hein, 2001).
8 They are from 5 to 10 μm in diameter and usually show negative crystal shape. Fluid inclusions
9 from type V veins are primary (in the sense of Roedder, 1984). They are randomly distributed
10 (Fig. 7b), up to 50 μm across, and elongated parallel to the ϵ axis of vesuvianite. Fluid inclusions
11 in both garnet and vesuvianite are two-phase (L+V) liquid-dominated aqueous inclusions
12 showing a degree of filling [$df = L/(L+V)$] of 0.8. In all the inclusions, the vapour phase has a
13 brownish to blackish unusual colour (Fig. 7c). Microthermometric measurements (Table 4) show
14 freezing temperatures between -66.1 and -55.8 $^{\circ}\text{C}$, with majority at -58.4 $^{\circ}\text{C}$. Eutectic
15 temperatures can not be recognised, but a liquid phase is observed at temperatures between –
16 53.9 and -32.5 $^{\circ}\text{C}$. These data reveal the presence of dissolved Ca^{2+} in addition to Na^{+} .
17 Hydrohalite melts between -28.7 and -18.3 $^{\circ}\text{C}$ (with majority at -24.3 $^{\circ}\text{C}$), and ice melts
18 between -13.9 and -5.9 $^{\circ}\text{C}$, with most measurements at -7.7 $^{\circ}\text{C}$. The homogenisation, always to
19 the liquid phase, ranges between 239.7 and 380.8 $^{\circ}\text{C}$, with most values at 286.7 $^{\circ}\text{C}$ (Fig. 8a and
20 Table 4).

21
22 Micro-Raman analyses performed on the gas bubbles always show spectra with well defined
23 peaks at 4127 , 4145 , 4157 , and 4163 cm^{-1} for molecular H_2 (Fig. 8b), and at 2918 cm^{-1} for CH_4
24 (not shown in Fig. 8b). Quantitative analyses (n. 13) reveal the presence of 78-90 mole % of H_2
25 and 22-10 mole % of CH_4 . The high-quality of the hydrogen Raman signal (Fig. 8b) suggests

1 that the gas density in the bubble should be in the range 0.01 - 0.005 g/cm³. Based on the
2 volume of the bubble relative to the whole inclusion, the H₂ + CH₄ content in the fluid can be
3 tentatively estimated between 1.0 and 0.4 mole %. All these data indicate that the fluid in the
4 inclusions is a complex H₂O-H₂-CH₄ mixture dominated by saline (6 wt % CaCl₂ + 6 wt % NaCl)
5 aqueous fluids (X_{H₂O} = 0.988) with minor H₂ (probably X_{H₂} = 0.010) and traces of CH₄ [X_{CH₄} =
6 0.002; H₂/(H₂+CH₄) = 0.86].

7

8 **Discussion**

9

10 *Tectono-metamorphic evolution*

11

12 Field relationships indicate that the boudins of the fine-grained rodingite derive from deformation
13 and disruption of a primary single dyke (Fig. 2). The local preservation of a relict subophitic
14 microstructure (Fig. 3b), of an igneous Ti-bearing clinopyroxene (Figs. 3d and 9a), and of a Cr-
15 bearing spinel (Figs. 3e and 9a) suggests a doleritic (basaltic) dyke protolith. This dyke was
16 intrusive into a tectonitic spinel lherzolite—as suggested by the presence in the hosting
17 serpentinite of peridotitic relics of Cr-rich spinel, clinopyroxene and orthopyroxene (bastite
18 pseudomorphs) (Fig. 9b)—flooring the Mesozoic Piemonte-Liguria oceanic basin.

19

20 Although both the basaltic dyke and the hosting peridotite do not preserve other evidence of
21 ocean-floor metamorphism (Fig. 9), it is highly probable that they experienced oceanic
22 rodingitisation and serpentinitisation. The rodingitisation should have been pervasive throughout
23 the dyke, as suggested by both the high modal amount of diopside and the lack of epidote *s.l.*
24 (see e.g., Schandl et al., 1989; O'Hanley, 1996).

25 Both serpentinites and rodingites subsequently experienced the Alpine orogenic cycle.

1

2 In serpentinites, during eclogite-facies conditions coarse-grained olivine + diopside + antigorite
3 + titanian-clinohumite ± chlorite developed in the rock matrix and chlorite + olivine + titanian-
4 clinohumite in type A veins. These minerals recrystallised to finer-grain size during a
5 deformation event, still at eclogite-facies conditions, responsible for the development of the S_{r-1}
6 foliation (Fig. 9b; e.g., Groppo and Compagnoni, 2007b and references therein). The diopside-
7 bearing veins (type B veins), which cut across S_{r-1} and are transposed by the S_r foliation, must
8 have formed during an early post-eclogite facies decompression stage (Fig. 9b). During the
9 development of the regional foliation (S_r), antigorite, chlorite, diopside, magnetite and, possibly,
10 olivine recrystallised and mostly acquired a preferred orientation (Fig. 9b). In the Zermatt-Saas
11 Unit, S_r is usually referred to the deformation processes active during the nappe emplacement
12 at greenschist-facies conditions (Borghini et al., 1996; Castelli et al., 1995; Li et al., 2004a).

13

14 The alteration of olivine and diopside to produce antigorite, and its recrystallisation on the S_{r+1}
15 crenulation cleavage plane, likely occurred during the subsequent cooling path (Fig. 9b). In the
16 Bellecombe serpentinite, such as in other serpentinites from the Piemonte Zone (Groppo and
17 Compagnoni, 2007b), this ductile deformation event was followed by a brittle one, accompanied
18 by the development of monomineralic talc, tremolite, or chrysotile veins (type C veins), which
19 clearly cut across S_{r+1} (Fig. 9b).

20 Unlike the interpretation of Li et al. (2004b, 2008) and Panseri et al. (2008), who considered
21 their boudins of rodingites with different mineral assemblages as derived from different protolith
22 composition, degree of rodingitisation, and/or Alpine metamorphic overprint, the studied
23 Bellecombe rodingite derives from a single basaltic dyke. Consequently, microstructural and
24 mineral relationships between the fine-grained rodingite and the different vein generations allow
25 us to reconstruct the whole tectono-metamorphic evolution and to suggest an alternative genetic

1 interpretation. Although a significant difference in rheology prevented rodingites from recording
2 in detail the ductile deformation shown by the hosting serpentinite, the same deformational and
3 metamorphic history is recorded by both fine-grained rodingite + rodingitic veins and hosting
4 serpentinite (Fig. 9). In particular, the microstructural evolution is characterised by the
5 development of mineral assemblages and pre-S_r, syn-S_r, pre-S_{r+1}, and post-S_{r+1} vein
6 generations (Fig. 9a).

7
8 Evidence for the eclogite-facies event is lacking in rodingite, as a consequence of an early
9 pervasive ocean-floor rodingitisation, that leached out some elements, especially Na. Thus, in
10 pervasively metasomatised dykes, common rodingitic minerals—such as grossular/andradite
11 garnet, diopside, vesuvianite, epidote, and chlorite— which are stable up to 3.5 GPa (Li et al.,
12 2007), occur instead of the typical high-pressure eclogite-facies index minerals, in particular
13 omphacite. In contrast, mafic rocks, which underwent only a small degree of ocean-floor
14 rodingitisation, during HP conditions can produce an eclogitic mineral assemblage (i.e.
15 almandine-rich garnet + Na-rich pyroxene; e.g. Evans et al., 1979; Dal Piaz et al., 1980;
16 Cimmino et al., 1981; Puga et al., 1999; Ferraris and Compagnoni, 2003; Li et al., 2007).

17
18 In the studied Bellecombe rodingite, mineral assemblages and mineral chemistries only slightly
19 changed during metamorphic evolution. The oldest rodingitic mineral assemblage, which is
20 microstructurally compatible, and therefore coeval, with the HP assemblage in the hosting
21 serpentinite, consists of grossular garnet + diopside + chlorite in the fine-grained rodingite and
22 of type I veins (Fig. 9a). During an early stage of decompression, the garnet composition in both
23 the fine-grained rodingite and the type II and III veins progressively enriched in the andradite-
24 component: during this process the progressive disappearance of diopside is counterbalanced
25 by the growth of chlorite (Fig. 9a). An increase in Fe³⁺, coupled with the chlorite growth, is

1 commonly found in strongly rodingitised rocks: it has been interpreted as due to chemical re-
2 equilibration under relatively high f_{O_2} (Hatzipanagiotou et al., 2003; Dubinska et al., 2004) by a
3 reaction such as: $21\text{Hed} + 1\text{Grs} + 4\text{O}_2 + 4\text{H}_2\text{O} = 8\text{Adr} + 1\text{Chl} + 18\text{SiO}_{2\text{aq}}$ (Li et al., 2008).
4 During the ductile deformation that produced S_r and during the formation of type IV veins that
5 post-date S_r , garnet became slightly enriched in the grossular-component, probably by a
6 reaction such as: $\text{Adr} + \text{Chl} + \text{Ca}^{2+} = \text{Grs} + \text{Di} + \text{H}_2\text{O}$ (Li et al., 2004b). During formation of type
7 V veins (Fig. 9a), the garnet of the fine-grained rodingite and of all the previous veins was partly
8 replaced by vesuvianite, possibly by a reaction such as: $\text{Grs} + \text{Di} + \text{H}_2\text{O} = \text{Ves} + \text{Chl}$ (Li et al.,
9 2004b). The latest deformation, which produced the S_{r+1} crenulation, is accompanied by the
10 recrystallisation of chlorite and by the formation of type VI veins filled with Fe-rich chlorite.
11
12 A complete P - T path of the Zermatt-Saas Unit, exposed to the south of the Aosta-Col de Joux-
13 Ranzola fault, is not yet available. Martin et al. (2008) concluded that the HP metamorphic peak
14 of the St. Marcel meta-ophiolites (Fig. 1) occurred at $550 \pm 60^\circ\text{C}$ and $2.1 \pm 0.3\text{ GPa}$ (Fig. 10).
15 Similar peak conditions ($T \sim 600^\circ\text{C}$, $P < 2.4\text{ GPa}$; Fig. 10) have been recently estimated for
16 meta-ophiolites of a Zermatt-Saas unit adjoining the UHP Lago di Cignana unit, exposed to the
17 north of the Aosta-Col de Joux-Ranzola fault (Groppo et al., 2009). A complete P - T path (see
18 Fig. 10) for serpentinites and associated rodingites from the Zermatt-Saas Zone has been
19 proposed by Li et al. (2004a, 2004b, 2008) for the Lichenbretter area, Swiss Western Alps.
20 These authors observed the local occurrence of a relict mesh microstructure in serpentinites
21 and of a Czo-Grs-Chl-Di mineral assemblage in the associated rodingites, both interpreted as
22 evidence of a low-grade ($P \cong 0.2\text{ GPa}$ and $T = 200^\circ\text{C}$) ocean-floor metamorphism. The mineral
23 assemblages antigorite + olivine + magnetite + diopside in serpentinites and grossular +
24 diopside + chlorite \pm andradite in rodingites are considered to have formed during the eclogite-
25 facies metamorphism at $P = 2.5 - 3.0\text{ GPa}$ and $T = 600 - 650^\circ\text{C}$, whereas the later

1 retrogressive recrystallisation during exhumation at $P = 0.9 - 1.2$ GPa and $T = 500 - 550$ °C.
2 After the nappe emplacement and the development of S_r ($T = 400-450$ °C; $P = 0.3-0.5$ GPa), a
3 late growth of vesuvianite occurred at sub-greenschist-facies conditions ($T \cong 300$ °C; $P \cong 0.2$
4 GPa). Because the whole orogenic evolution estimated by Li et al. (2004a, 2004b, 2008) is
5 consistent with that of the studied rodingites and serpentinites (Fig. 9), we can reasonably
6 assume that the Bellecombe lithologies may have experienced a similar P - T path, in particular
7 during the exhumation history.

8

9 *Origin and preservation of the reducing fluid*

10

11 Two possible origins, internal vs. external, can be envisaged for the H_2 -bearing brine with traces
12 of CH_4 present during the vesuvianite growth. An internal origin is less probable for lacking
13 evidence of mineral dehydration during the vesuvianite growth (Fig. 9a). On the contrary, an
14 external origin, connected to the hydration of the hosting ultramafic rocks during exhumation
15 (see below), is more likely because significant concentrations of CH_4 and H_2 can be promoted
16 by the extremely reducing conditions existing at the serpentinisation front (e.g., Frost, 1985). In
17 particular, Ca-rich aqueous solutions with variable salinity and amounts of H_2 and CH_4 , found in
18 a number of serpentinites and associated rodingites, were interpreted as related to
19 serpentinisation and rodingitisation processes (Schandl et al., 1990; Mittwede and Schandl,
20 1992; Peretti et al., 1992; Kelley, 1996; Palandri and Reed, 2004; Frost and Beard, 2007;
21 Murzin and Shanina, 2007). The H_2 enrichment in serpentinite-derived fluids seems to be due to
22 hydration reactions during serpentinisation such as $2FeO$ (Ol, Px) + $H_2O = 2Fe_2O_3$ (Hem) + H_2
23 (Palandri and Reed, 2004), $6Fe_2SiO_4$ (Fa) + $7H_2O = 3Fe_3Si_2O_5(OH)_4$ (Fe-Srp) + Fe_3O_4 (Hem) +
24 H_2 (Frost, 1985), $3Fe_2SiO_4$ (Fa) + $2H_2O = 2Fe_3O_4$ (Mag) + $3SiO_2$ + $2H_2$, and Cr -Spl + Fe^{3+} + H_2O
25 = ferrit-Chr + Mag + Al^{3+} + H_2 (Iyer et al., 2008). The presence of dissolved CO_2 in the

1 circulating fluids and/or the presence of carbonates are necessary to produce CH₄ in the
2 presence of H₂ during serpentinisation. An abiogenic methane generation (Sherwood Lollar et
3 al., 1993; Kelley and Früh-Green, 1999) has been obtained at temperatures higher than 300 °C
4 by 1) the Fischer-Tropsch reaction: CO₂ + 4H₂ = CH₄ + 2H₂O (e.g., Berndt et al., 1996), and 2)
5 via reactions such as: Ol + H₂O + C (or CO₂) = Mag + Srp + CH₄ + Brc + H₂ (Abrajano et al.,
6 1990) or 4H₂ + CaCO₃ = CH₄ + CaO + 2H₂O (Scott et al., 2004). Fe-Ni alloys seem to catalyse
7 the formation of methane via the reaction: HCO₃⁻ + 4H₂ = CH₄ + OH⁻ + 2H₂O (Horita and Berndt,
8 1999; McCollom and Seewald, 2001).

9

10 Although there is a general agreement on the presence of reduced fluids in ophiolite complexes
11 undergoing serpentinisation (e.g.: Frost and Beard, 2007 and references therein), H₂ has been
12 detected only very rarely (Peretti et al., 1992; Murzin and Shanina, 2007; Normand and William-
13 Jones, 2007). As evident from experimental studies (e.g. Hall et al., 1991; Mavrogenes and
14 Bodnar, 1994), its rarity is probably due to the tendency of H₂ to diffuse out of the inclusions.
15 However, in the Bellecombe rodingite, H₂ has been detected in both garnet and vesuvianite. Its
16 preservation might be due: i) to the very high amount of H₂ originally present in the fluid, or ii) to
17 the lack of the fluid inclusion re-equilibration due to their relatively young trapping at low-*P* and
18 low-*T* conditions. The same amount of H₂ measured in fluid inclusions from both garnet and
19 vesuvianite, two minerals with different crystallographic structure and elastic properties, appears
20 to be in favour of the second hypothesis.

21

22 *Characterisation of the late-Alpine rodingitisation event*

23

24 Because the precise molar volume of the H₂-CH₄ mixture is unknown, a fluid isochore has been
25 calculated in the simplified H₂O-NaCl-CaCl₂ system (see dashed grey line in Fig. 10).

1 Nevertheless, this isochore gives entrapment pressures too low for the estimated late-Alpine
2 greenschist-facies conditions (Fig. 10). The addition to the H₂O-NaCl-CaCl₂ system of 1 mole %
3 of H₂—based tentatively on the volume of the gas bubble within fluid inclusions (see above)—
4 considerably increases the fluid density (from 0.81 to 0.87 g/cm³). The resulting isochore (thick
5 grey line in Fig. 10) is much steeper and indicates trapping pressures of 0.22 GPa (at 400 °C),
6 which are consistent with the *P-T* evolution of the Bellecombe rodingites (Fig. 10). At the
7 inferred *P-T* conditions, such a fluid composition is indicative of a $f_{\text{O}_2} = -2$ ($\log f_{\text{O}_2} = -30.59$) at
8 QFM conditions and of a carbon activity (a_{C}) lower than 0.001, otherwise only CH₄ would be
9 present and a Ca-rich garnet would be the stable phase instead of vesuvianite (Christophe-
10 Michel-Lévy, 1960; Ito and Arem, 1970).

11
12 The present study reveals that the late growth of vesuvianite in type V veins and, most likely, in
13 the fine-grained rodingite as well, was promoted by a rodingitisation process, active during a
14 late stage of the Alpine metamorphic evolution, which occurred in the presence of
15 serpentinisation-derived fluids. The reduced fluid responsible for the rodingitisation process was
16 generated through the late serpentinisation of the metamorphic olivine in the hosting
17 serpentinites: this interpretation is in agreement with the *P-T* conditions estimated for the type V
18 vein formation, which intersect the olivine-out reaction (Fig. 10; Li et al., 2004a). In the Western
19 Alps, a rodingitisation event at similar *P-T* conditions (0.3-0.4 GPa, 300-400 °C) has been
20 estimated by Castelli et al. (1995) for rodingites from the Balangero asbestos mine, Lanzo
21 Massif (Fig. 10). This event, accompanied by the growth of native iron and Ni-Fe alloys,
22 occurred during the greenschist-facies serpentinisation of the Balangero ultramafics (Rossetti
23 and Zucchetti, 1988a, 1988b). A similar serpentinisation process, occurred during exhumation,
24 has been also reported from the Lichenbretter serpentinites of the Zermatt-Saas Unit ($P \cong 0.2$

1 GPa and $T > 375$ °C; Li et al., 2004a) as well as from other ophiolitic complexes involved in
2 orogenic belts (e.g., Mittwede and Schandl, 1992; Li et al., 2007).

3

4 **Conclusions**

5

6 This study has demonstrated that the boudins of fine-grained rodingite and the hosting antigorite
7 serpentinite from Bellecombe were derived, respectively, from a former basaltic dyke and from
8 the hosting spinel lherzolites flooring the Mesozoic Piemonte-Liguria ocean. After a pervasive
9 ocean-floor metamorphism, both lithologies were involved in the Alpine orogeny. Their tectono-
10 metamorphic evolution was characterised by a successive events of veining and ductile
11 deformation, which record an early peak at eclogite-facies conditions, followed by a
12 decompression and a final cooling at greenschist- to sub-greenschist-facies conditions. Such
13 evolution has been inferred from mineral assemblages developed not only in the serpentinite,
14 but also in the rodingites. In particular, grossular garnets, associated to chlorite and diopside,
15 formed at HP conditions, andradite-rich garnets and chlorite—but not diopside—were stable
16 during decompression, and a new generation of grossular-rich garnet formed again at
17 greenschist-facies conditions. The final cooling was accompanied by the garnet destabilisation
18 and the growth of vesuvianite and chlorite.

19

20 The fluid inclusion study of rodingites has revealed that the growth of vesuvianite at $P = 0.22$
21 GPa and $T = 400$ °C was promoted by the influx of H_2 -bearing brines with traces of CH_4 . This
22 reducing fluid was generated in the hosting serpentinites from the late-Alpine serpentinisation of
23 early-Alpine metamorphic olivine. This implies that the Bellecombe rodingites experienced at
24 least two rodingitisation events: a first one, which likely occurred during ocean-floor

1 metamorphism, and a second one, which took place during late stages of the Alpine tectono-
2 metamorphic evolution.

3

4 **Acknowledgments**

5

6 A. Facchinelli, P. Rossetti, and C. Trossarelli are gratefully acknowledged for constructive
7 discussions. A careful and constructive review by G. Piccardo has been most helpful and is
8 highly appreciated. This work was financially supported by grants from the University of Torino
9 to R.C., and from the University of Siena to M.L.F. (PAR 2006). The Raman facility in Siena was
10 provided by the Italian Program for Research in Antarctica (P.N.R.A.), and the Raman facility in
11 Torino by the Interdepartmental Center "G. Scansetti" for Studies on Asbestos and Other Toxic
12 Particulates, funded by the Compagnia di San Paolo, Torino. We thank Y. Dilek for his review
13 and copy-editing of the final manuscript.

1 **References**

2

3 Abrajano, T. A., Sturchio, N. C., Kennedy, B. M., Lyon, G. L., Muehlenbachs, K., and Bohlke, J.
4 K., 1990, Geochemistry of reduced gas related to serpentinisation of the Zambales ophiolite,
5 Philippines: *Applied Geochemistry*, v. 5, 625-630.

6 Bakker, R. J., 2003, Package FLUIDS 1. Computer programs for analysis of fluid inclusion data
7 and for modelling bulk fluid properties: *Chemical Geology*, v. 194, 3-23.

8 Bakker, R. J., and Brown, P., 2003, Computer modelling in fluid inclusion research. *In* Fluid
9 inclusions: analysis and interpretation (I. Samson, A. Anderson, D. Marshall, eds):
10 Mineralogical Association of Canada Short Course Series, v. 32, 175-212.

11 Berndt, M. E., Allen, D. E., and Seyfried, W. E., 1996, Reduction of CO₂ during serpentinization
12 of olivine at 300 °C and 500 bar: *Geology*, v. 24, 351–354.

13 Bezzi, A., and Piccardo, G. B., 1969, Studi petrografici sulle formazioni ofiolitiche dell'Appennino
14 Ligure. Nota XII. Le rodingiti di Carro (La Spezia): *Bollettino della Società Geologica Italiana*,
15 v. 88, 645-687 (In Italian).

16 Borghi, A., Compagnoni, R., and Sandrone, R., 1996, Composite P-T paths in the Internal
17 Penninic massifs of the Western Alps: petrological constraints to their thermo-mechanical
18 evolution: *Eclogae geologicae Helvetiae*, v. 89, 345-367.

19 Castelli, D., Rolfo, F., and Rossetti, P., 1995, Petrology of ore-bearing rodingite veins from the
20 Balangero asbestos mine (Western Alps): *Bollettino del Museo Regionale di Scienze
21 Naturali di Torino*, v. 13, 153-189.

22 Christophe-Michel-Lévy, M., 1960, Reproduction artificielle de l'idocrase: *Bulletin de la Société
23 Française de Minéralogie et de Cristallographie*, v. 83, 23-25 (in French).

24 Cimmino, F., Messiga, B., and Piccardo, G., 1981, Le caratteristiche paragenetiche dell'evento
25 eo-alpino di alta pressione nei diversi sistemi (pelitici, femici, ultrafemici) delle ofioliti

- 1 metamorfiche del Gruppo di Voltri (Liguria Occidentale): Rendiconti della Società Italiana di
2 Mineralogia e Petrologia, v. 37, 419-446 (in Italian).
- 3 Coleman, R. G., 1977, Ophiolites, minerals and rocks. Springer-Verlag, Berlin/Heidelberg,
4 Germany, 229 p.
- 5 Dal Piaz, G. V., 1967, Le "granatiti" (rodingiti l.s.) nelle serpentine delle Alpi occidentali italiane:
6 Memorie della Società Geologica Italiana, v. 6, 263-315 (in Italian).
- 7 Dal Piaz, G. V., Di Battistini, G., Gosso, G., and Venturelli, G., 1980, Rodingitic gabbro dykes
8 and rodingitic reaction zones in the upper Valtournanche-Breuil area, Piemonte ophiolite
9 nappe, Italian Western Alps: Archive Scientifique de Genève, v. 33, 161-179.
- 10 Dal Piaz, G. V., and Grasso, F. 1967, Le rodingiti s.l. nelle gallerie "Petit Monde" della
11 autostrada Quincinetto-Aosta: Bollettino della Società Geologica Italiana, v. 86, 395-401 (in
12 Italian).
- 13 Dietrich, H., Koller, F., Richter, W., and Kiesl, W., 1986, Petrologie und Geochemie des
14 Rodingit-Vorkommens vom Isnitzfall (Dorfertal, Hohe Tauern): Schweizerische
15 Mineralogische und Petrographische Mitteilungen, v. 66, 163-192 (in German).
- 16 Downs, R. T., 2006, The RRUFF Project: an integrated study of the chemistry, crystallography,
17 Raman and infrared spectroscopy of minerals: Program and Abstracts of the 19th General
18 Meeting of the International Mineralogical Association in Kobe, Japan. O03-13
- 19 Dubińska, E., Bylina, P., and Kozłowski, A., 2004, Garnets from lower Silesia rodingites:
20 constraints from their chemistry: Mineralogical Society of Poland, Special Paper, v. 24, 135-
21 139.
- 22 Evans, B. W., Trommsdorff, V., and Richter, W., 1979, Petrology of an eclogite-metarodingite
23 suite at Cima di Gagnone, Ticino, Switzerland: American Mineralogist, v. 64, 15-31.
- 24 Ferraris, C., and Compagnoni, R., 2003, Metamorphic evolution and significance of a
25 serpentized peridotite slice within the Eclogitic Micaschist Complex of the Sesia-Zone

1 (Western Alps-Italy): Schweizerische Mineralogische und Petrographische Mitteilungen, v.
2 83, 3-13.

3 Fettes, D., and Desmons, J. (eds), 2007, Metamorphic rocks. A classification and glossary of
4 terms. Recommendations of the International Union of Geological Sciences,
5 Subcommission on the Systematics of Metamorphic Rocks. Cambridge University Press,
6 Cambridge, U.K., 244 p.

7 Fontana, E., Panseri, M., and Tartarotti, P., 2008, Oceanic relict textures in the Mount Avic
8 serpentinites, Western Alps: *Ofioliti*, v. 33, 105-118.

9 Frost, B. R., 1985, On the stability of sulfides, oxides, and native metals in serpentinite: *Journal*
10 *of Petrology*, v. 26, 31-63.

11 Frost, B.R., and Beard, J. S., 2007, On silica activity and serpentinisation: *Journal of Petrology*,
12 v. 48, 1351-1368.

13 Giardino, M., 1996, Aspetti metodologici e problemi cartografici dello studio di deformazioni
14 superficiali nella Media Valle d'Aosta: *Il Quaternario*, v. 9, 227-232, (in Italian).

15 Groppo, C., and Compagnoni, R., 2007a, Ubiquitous fibrous antigorite veins from the Lanzo
16 Ultramafic Massif, Internal Western Alps (Italy): characterisation and genetic conditions:
17 *Periodico di Mineralogia*, v. 76, 169-181.

18 Groppo, C., and Compagnoni, R., 2007b, Metamorphic veins from the serpentinites of the
19 Piemonte Zone, Western Alps, Italy: a review: *Periodico di Mineralogia*, v. 76, 127-153.

20 Groppo, C., Beltrando, M., and Compagnoni, R., 2009, The P-T path of the ultra-high pressure
21 Lago di Cignana and adjoining high-pressure meta-ophiolitic units: insights into the
22 evolution of the subduction Tethyan slab: *Journal of Metamorphic Geology*, v. 27, 207-231.

23 Hall, D. L., Bodnar, R. J., and Craig, J. R., 1991, Evidence for postentrapment diffusion of
24 hydrogen into peak metamorphic fluid inclusions from the massive sulfide deposits at
25 Ducktown, Tennessee: *American Mineralogist*, v. 76, 1344–1355.

- 1 Hatzipanagiotou, K, Tsikouras, B., Migiros, G., Gartzos, E., and Serelis, K., 2003, Origin of
2 rodingites in ultramafic rocks from Lesvos Island (NE Aegean, Greece): *Ophioliti*, v. 28, 13-23.
- 3 Hey, M. H., 1954, A new review of the chlorites: *Mineralogical Magazine*, v. 30, 277-292.
- 4 Honnorez, J., and Kirst, P., 1975, Petrology of rodingites from equatorial Mid-Atlantic fracture
5 zones and their geotectonic significance: *Contributions to Mineralogy and Petrology*, v. 49,
6 233-257.
- 7 Horita, J., and Berndt, M. E., 1999, Abiogenic methane formation and isotopic fractionation
8 under hydrothermal conditions: *Science*, v. 285, 1055-1057.
- 9 Ito, J., and Arem, J. E., 1970, Idocrase: synthesis, phase relations and crystal chemistry:
10 *American Mineralogist*, v. 55, 880-901.
- 11 Iyer, K., Austrheim, H., John, T., and Jamtveit, B., 2008, Serpentinization of the oceanic
12 lithosphere and some geochemical consequences: constraints from the Leka Ophiolite
13 Complex, Norway: *Chemical Geology*, v. 249, 66-90.
- 14 Kelley, D. S., 1996, Methane-rich fluids in the oceanic crust: *Journal of Geophysical Research*,
15 v. 101, 2943-2962.
- 16 Kelley, D. S., and Früh-Green, G., 1999, Abiogenic methane in deep-seated mid-ocean ridge
17 environments: insights from stable isotope analyses: *Journal of Geophysical Research*, v.
18 104, 10439-10460.
- 19 Kretz, R., 1983, Symbols for rock-forming minerals: *American Mineralogist*, v. 68, 277-279.
- 20 Li, X. P., Rahn, M., and Bucher, K., 2004a, Serpentinites of the Zermatt-Saas ophiolite complex
21 and their texture evolution: *Journal of Metamorphic Geology*, v. 22, 159-177.
- 22 Li, X. P., Rahn, M., and Bucher, K., 2004b, Metamorphic processes in rodingites of the Zermatt-
23 Saas ophiolites: *International Geology Review*, v. 46, 28-51.

- 1 Li, X. P., Rahn, M., and Bucher, K., 2008, Eclogite facies metarodingites – phase relations in the
2 system $\text{SiO}_2\text{-Al}_2\text{O}_3\text{-Fe}_2\text{O}_3\text{-FeO-MgO-CaO-CO}_2\text{-H}_2\text{O}$: an example from the Zermatt-Saas
3 ophiolite: *Journal of Metamorphic Geology*, v. 26, 347-364.
- 4 Li, X. P., Zhang, L., Wei, C., Ai, Y., and Chen, J., 2007, Petrology of rodingite derived from
5 eclogite in western Tianshan, China: *Journal of Metamorphic Geology*, v. 25, 363-382.
- 6 Lindsley, D. H., and Anderson, D. J., 1983, A two-pyroxene thermometer. Proceedings of 13th
7 Lunar and Planetary Science Conference: *Journal of Geophysical Research*, v. 88
8 Supplement, 887-906.
- 9 Martin, S., Rebay, G., Kienast, J. R., and Mével, C., 2008, An eclogitised oceanic palaeo-
10 hydrothermal field from the St. Marcel Valley (Italian Western Alps): *Ofioliti*, v. 33, 49-63.
- 11 Mavrogenes, J. A., and Bodnar, R. J., 1994, Hydrogen movement into and out of fluid inclusions
12 in quartz: Experimental evidence and geologic implications: *Geochimica et Cosmochimica*
13 *Acta*, v. 58, 141–148.
- 14 McCollom, T. M., and Seewald, J. S., 2001, A reassessment of the potential for reduction of
15 dissolved CO_2 to hydrocarbons during serpentinization of olivine: *Geochimica et*
16 *Cosmochimica Acta*, v. 65, 3769-3778.
- 17 Mittwede, S. K., and Schandl, E. S., 1992, Rodingites from the southern Appalachian Piedmont,
18 South Carolina, USA.: *European Journal of Mineralogy*, v. 4, 7-16.
- 19 Murzin, V. V., and Shanina, S. N., 2007, Fluid regime and origin of gold-bearing rodingites from
20 the Karabash alpine-type ultrabasic massif, Southern Ural: *Geochemistry International*, v.
21 45, 998-1011.
- 22 Normand, C., and Williams-Jones, A. E., 2007, Physicochemical conditions and timing of
23 rodingite formation: evidence from rodingite-hosted fluid inclusions in the JM Asbestos mine,
24 Asbestos, Québec: *Geochemical Transactions*, v. 8:11. doi: 10.1186/1467-4866-8-11.
- 25 O’Hanley, D. S., 1996, *Serpentinites*. Oxford Univ. Press, New York, U.S.A., 277 p.

- 1 O'Hanley, D. S., Schandl, E. S., and Wicks, F. J., 1992, The origin of rodingites from Cassia,
2 British Columbia, and their use to estimate T and P (H₂O) during serpentinisation:
3 *Geochimica et Cosmochimica Acta*, v. 56, 97-108.
- 4 Palandri, J. L., and Reed, M. H., 2004, Geochemical models of metasomatism in ultramafic
5 systems: serpentinization, rodingitization, and sea floor carbonate chimney precipitation:
6 *Geochimica et Cosmochimica Acta*, v. 68, 1115-1133.
- 7 Panseri, M., Fontana, E., and Tartarotti, P., 2008, Evolution of rodingitic dykes: metasomatism
8 and metamorphism in the Mount Avic serpentinites (Alpine ophiolites, Southern Aosta
9 Valley): *Ofioliti*, v. 33, 165-185.
- 10 Peretti, A., Dubessy, J., Mullis, J., Frost, R. B., and Trommsdorff, V., 1992, Highly reducing
11 conditions during Alpine metamorphism of the Malenco peridotite (Sondrio, northern Italy)
12 indicated by mineral paragenesis and H₂ in fluid inclusions: *Contributions to Mineralogy and*
13 *Petrology*, v. 112, 329-340.
- 14 Piccardo, G. B., Messiga, B., and Cimmino, F., 1980, Antigoritic serpentinites and rodingites of
15 the Voltri Massif: some petrological evidences for their evolutive history: *Ofioliti*, v. 5, 111-
16 114.
- 17 Puga, E., Nieto, J. M., Díaz de Federico, A., Bodinier, J. L., and Morten, L., 1999, Petrology and
18 metamorphic evolution of ultramafic rocks and dolerite dykes of the Betic Ophiolitic
19 Association (Mulhacén Complex, SE Spain): evidence of eo-Alpine subduction following an
20 ocean-floor metasomatic process: *Lithos*, v. 49, 23-56.
- 21 Roedder, E., 1984, Fluid inclusions (P. Ribbe, ed). *Review in Mineralogy*, 12. Mineralogical
22 Society of America, Washington, D.C., U.S.A., 678 p.
- 23 Rolfo, F., Compagnoni, R., and Tosoni, D., 2004, Geology and petrology of the Austroalpine
24 Châtillon Slice, Aosta Valley, Western Alps: *Geodinamica Acta*, v. 17, 91-105.

- 1 Rösli, U., 1988, Geochemische und mineralogische Untersuchungen an Metarodingiten. Ph.D.
2 Thesis, ETH Zürich (in German).
- 3 Rösli, U., Hoernes, S., and Köppel, V., 1991, Isotope data of metarodingites and associated
4 rocks from the Lanzo and the Bracco ophiolitic massifs: indications on the evolution of the
5 Alpine-type ultramafic-mafic complexes: Schweizerische mineralogische und
6 petrographische Mitteilungen, v. 71, 125-141.
- 7 Rossetti, P., and Zucchetti, S., 1988a, Early-alpine ore parageneses in the serpentinites from
8 the Balangero asbestos mine and Lanzo Massif (Internal Western Alps): Rendiconti della
9 Società Italiana di Mineralogia e Petrologia, v. 43, 139-149.
- 10 Rossetti, P., and Zucchetti, S., 1988b, Occurrence of native iron, Fe-Co and Ni-Fe alloys in the
11 serpentinite from the Balangero asbestos mine (Western Italian Alps): Ofioliti, v. 13, 43-56.
- 12 Schandl, E. S., O'Hanley, D. S., and Wicks, F. J., 1989, Rodingites in serpentinitized ultramafic
13 rocks of the Abitibi Greenstone Belt, Ontario: Canadian Mineralogist, v. 27, 579-591.
- 14 Schandl, E. S., O'Hanley, D. S., Wicks, F. J., and Kyser, T. K., 1990, Fluid inclusions in
15 rodingite: a geothermometer for serpentinisation: Economic Geology, v. 85, 1273-1276.
- 16 Scott, H. P., Hemley, R. J., Mao, H., Herschbach, D. R., Fried, L. E., Howard, W. M., and
17 Bastea, S., 2004, Generation of methane in the Earth's mantle: *in situ* high pressure-
18 temperature measurements of carbonate reduction: PNAS, v. 101, 14023-14026.
- 19 Sherwood Lollar, B., Frapé, S. K., Weise, S. M., Fritz, P., Macko, S. A., and Welhan, J. A.,
20 1993, Abiogenic methanogenesis in crystalline rocks: Geochimica et Cosmochimica Acta, v.
21 57, 5087-5097.
- 22 Thayer, T. P., 1966, Serpentinization considered as a constant-volume metasomatic process:
23 American Mineralogist, v. 51, 685-710.
- 24 Ulmer, P., 1986, NORM-Program for cation and oxygen mineral norms. Computer Library,
25 Institut für Mineralogie und Petrographie, ETH-Zentrum, Zürich, Switzerland.

- 1 van den Kerkhof, A. M., and Hein, U. F., 2001, Fluid inclusion petrography: *Lithos*, v. 55, 27-47.
- 2 Wares, R. P., and Martin, R. F., 1980, Rodingitization of granite and serpentinite in the Jeffrey
- 3 mine, Asbestos, Quebec: *Canadian Mineralogist*, v. 18, 231-240.
- 4

1 FIGURES

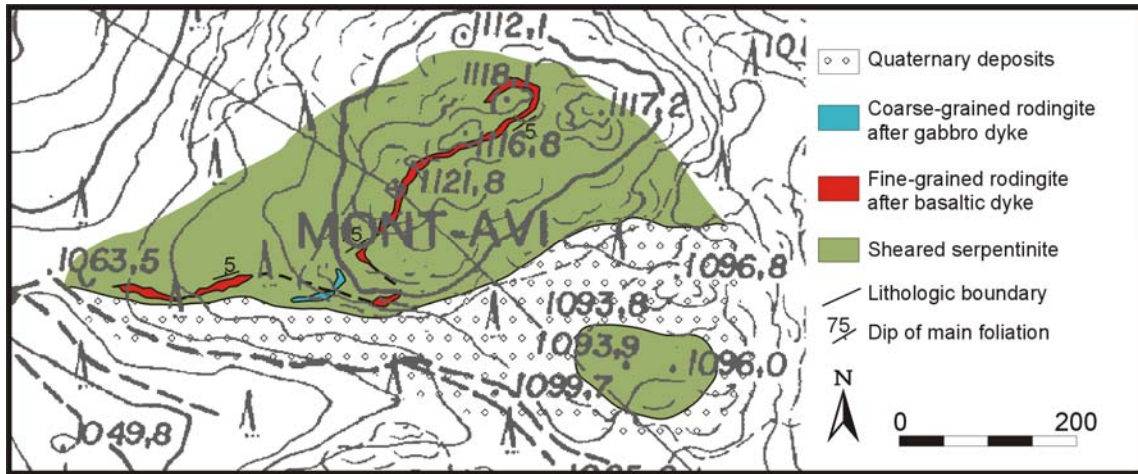


2
 3 FIG. 1. Tectonic sketch-map of the northwestern Alps (from Rolfo *et al.* 2004): Southalpine
 4 system (SA), undifferentiated. 2: Canavese Zone (CA). 3: Austroalpine system; 3a: Roisan (R)
 5 and Mt. Dolin (D) Mesozoic cover and undifferentiated mylonites; 3b: Units with prevailing pre-
 6 Alpine amphibolite- to granulite-facies metamorphism: Valpelline Series (VP), Second dioritic-
 7 kinzigitic Zone (DK), Vasario (VA) klippe; 3c: Units with Alpine eclogite-facies overprint: Eclogitic
 8 Micaschists Complex (EMC) of the Sesia Zone, and tectonic slices of Mt. Emilius (E), Glacier-
 9 Rafray (GR), Tour Ponton (TP), Santanel (S), Châtillon (CH), Etirol-Levaz (EL), Perrière (P),
 10 Grun (G) and Eaux Rousses (ER); 3d: Units lacking Alpine eclogite-facies overprint: Gneiss
 11 Minuti Complex (GMC) of the Sesia Zone, and thrust sheets of Dent Blanche (DB), M. Mary

1 (MM), Pilonnet (PI), and Verres (V); 3e: thrust sheets of the Rocca Canavese Unit. 4-6: Penninic
2 Zone. 4: Piemonte Zone: 4a1: units characterised by epidote blueschist-facies overprint; 4a2:
3 units characterised by eclogite-facies overprint; 4b: Ultramafic Lanzo massif (LA); 5: "Internal
4 Crystalline Massifs"; 5a: Upper Penninic units with Alpine eclogite-facies overprint: Gran
5 Paradiso (GP), Monte Rosa (MR) and Arcesina-Brusson (AB). 5b: Intermediate Penninic units
6 with Alpine epidote blueschist-facies overprint: Gran San Bernardo nappe (SB) -
7 undifferentiated - and Camughera-Moncucco Zone (CM). 6: Outer Penninic Valais units and
8 Sion-Courmayeur Zone, undifferentiated. 7: Helvetic-Ultrahelvetic system; 7a: Ultrahelvetic
9 cover nappes and M. Chetif massif, undifferentiated; 7b: Helvetic "External Crystalline Massifs"
10 with very low grade Alpine overprint: Mont-Blanc massif (MB). 8: Post-orogenic Oligocene
11 magmatic rocks: Brosso-Traversella (BT) and Valle del Cervo (C) intrusions. Tectonic
12 lineaments: FP: Penninic front, SC: Sempione line, CL: Canavese line, AJR: Aosta-Colle di
13 Joux-Colle della Ranzola fault system. Locations of rodingites described in previous papers and
14 in this study: dots, Dal Piaz & Grasso (1967); square, Dal Piaz *et al.* (1980); diamond, Li *et al.*
15 (2004b, 2008); triangle, Panseri *et al.* (2008); star, this study.

16

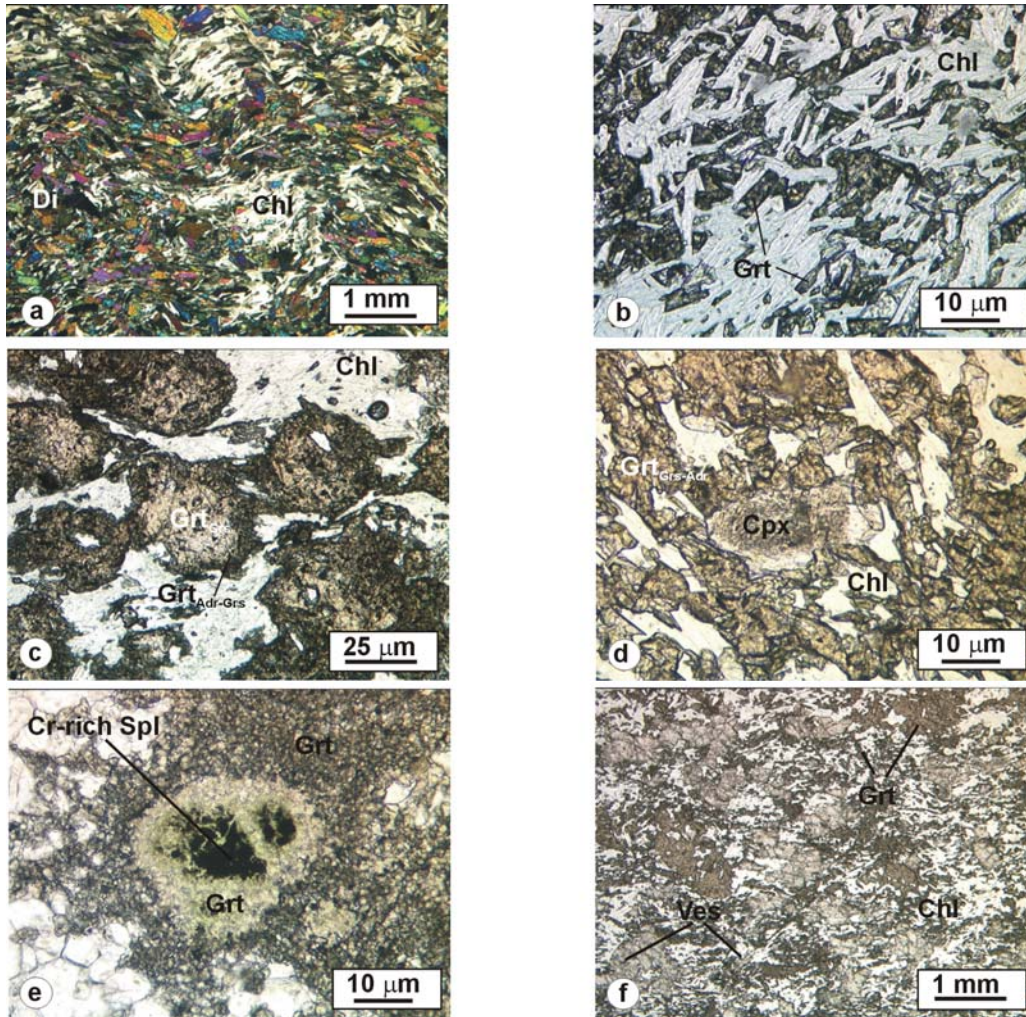
17



1

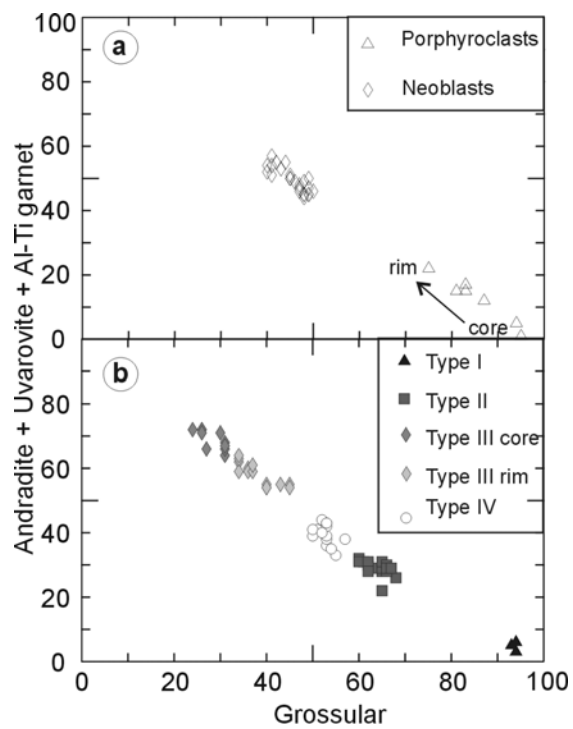
2

3 FIG. 2. Geological map of the Mont-Avi area, East of Bellecombe, Italy.

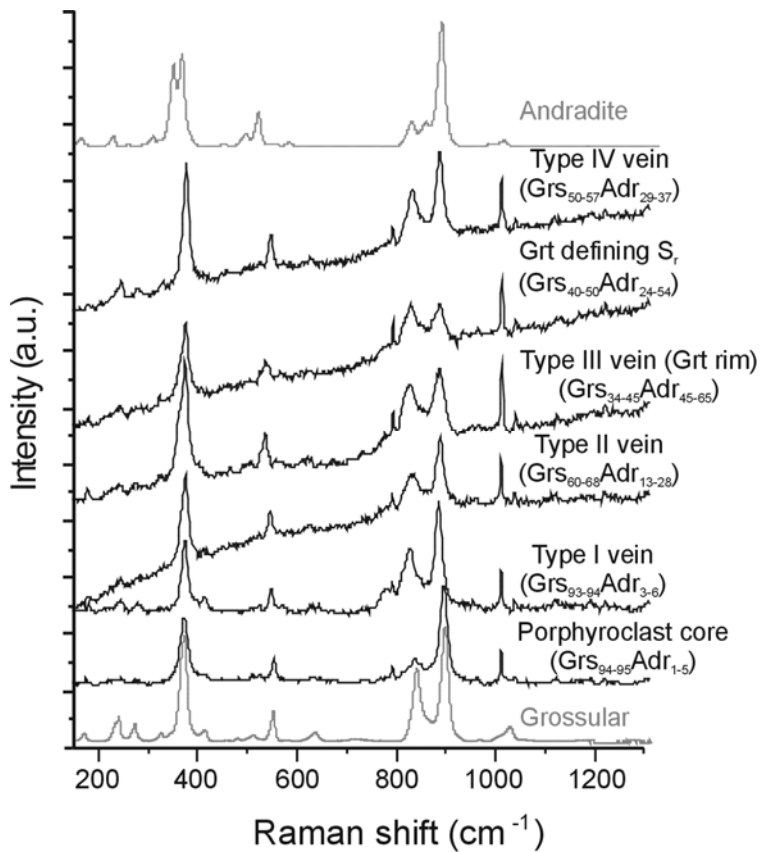


1
2 FIG. 3. Photomicrographs of the Bellecombe rodingites. a) Fine-grained rodingite showing a
3 crenulated S_r foliation defined by diopside and chlorite. Sample OF2379, Crossed Polars (CP).
4 b) Relict subophitic microstructure with lath-shaped garnets after magmatic plagioclase. Sample
5 OF2379, Plane Polarised Light (PPL). c) Porphyroclastic garnet wrapped around by the S_r and
6 showing a grossular core (light-grey) and a fine-grained andradite-grossular rim (dark-grey).
7 Sample OF2367, PPL. d) Diopside, after magmatic clinopyroxene, with segregation lamellae of
8 ilmenite in the core. The crystal is oblique to the main foliation defined by chlorite and fine-
9 grained andraditic garnet. Sample OF2378, PPL. e) Aggregate of green uvarovitic garnet
10 replacing a Cr-rich spinel. The uvarovite component rapidly decreases away from the spinel.

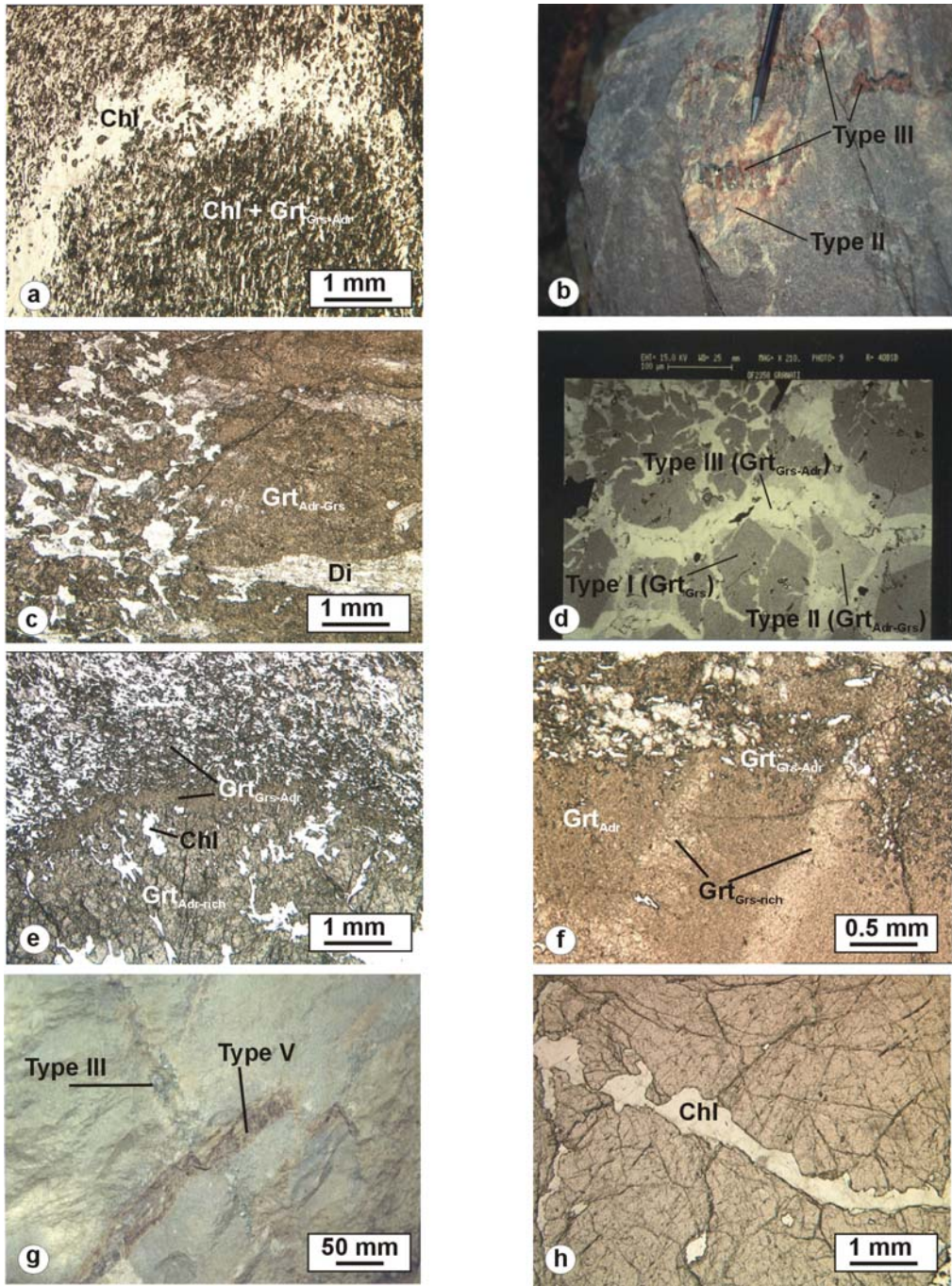
- 1 Sample OF2374, PPL. f) Vesuvianite (light-grey) partly replacing both porphyroclastic and fine-
- 2 grained (syn-S_r) garnet (dark-grey). Sample OF2378, PPL.



1
 2 FIG. 4. Chemical compositions of garnet plotted in the grossular-(andradite+uvarovite+Ti-Al
 3 garnet) diagram. a) garnets from both coarse-grained and fine-grained rodingites; b) garnets
 4 from the different vein generations.

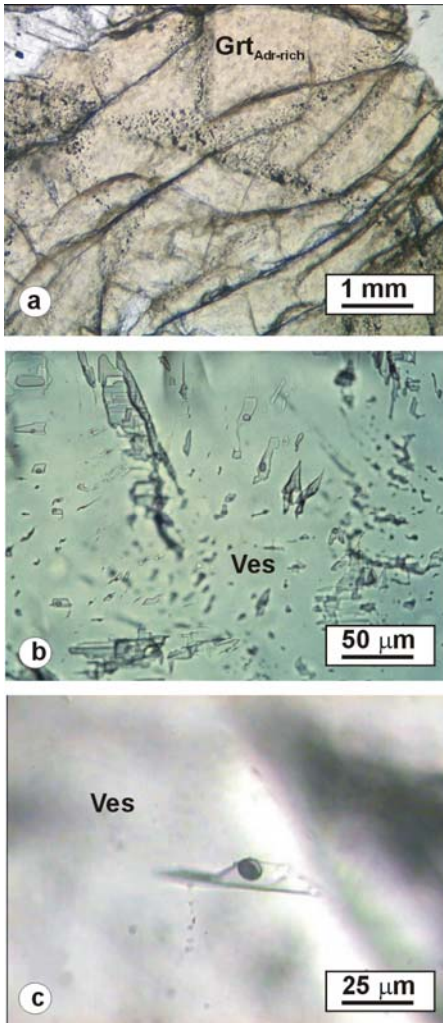


1
 2 FIG. 5. Representative Raman spectra of the different generations of garnet recognised in the
 3 Bellecombe rodingites and associated veins. The peaks around 550, 830 and 890 cm^{-1} ,
 4 sensitive to the grossular and andradite contents, shift towards lower values with the increase in
 5 the andraditic component, as evident from the comparison between pure grossular (R040066 of
 6 the RRUFF project; Downs, 2006) and pure andradite (R060326 of the RRUFF project; Downs,
 7 2006) spectra (in grey).

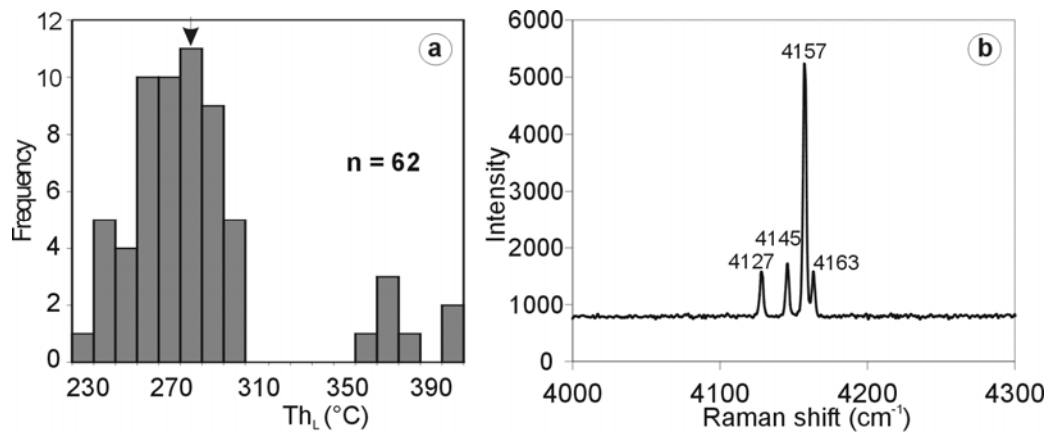


1
 2 FIG. 6. Images of the rodingitic veins cutting the fine-grained rodingite from Bellecombe. a)
 3 Photomicrograph of folded monomineralic Chl vein (type I). The axial plane foliation of the fold is
 4 parallel to the S_r defined by grossular-andraditic garnet and chlorite. Sample OF2372, PPL. b)
 5 Outcrop of fine-grained rodingite showing deformed type III (Chl + Grt) vein cutting type II (Di +

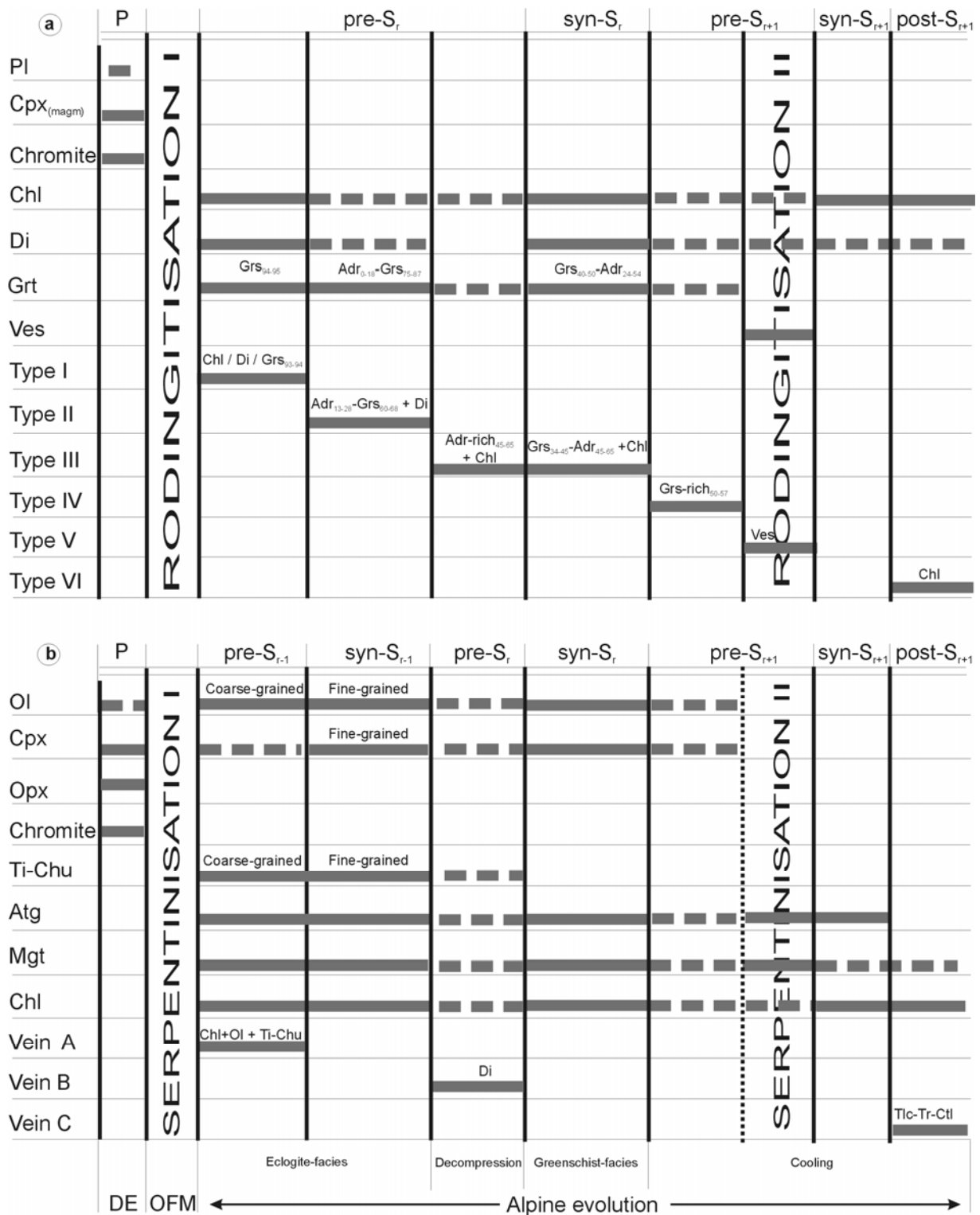
1 Grt) vein. c) Photomicrograph of a coarse-grained type II vein that consists of andraditic-
2 grossular garnet and diopside grown perpendicular to the vein selvages. Sample OF2366, PPL.
3 d) Back scattered electron image of a grossular garnet from a type I vein cut by type II veins
4 with andraditic-grossular garnet, in its turn cut by type III veins with grossular-andraditic garnet.
5 Sample OF2358. e) Photomicrograph of a coarse-grained andradite-rich garnet (Grt_{Adr}) from
6 type III vein rimmed by grossular-andradite ($\text{Grt}_{\text{Grs-Adr}}$) with the same composition as the fine-
7 grained garnet defining S_r in the hosting rodingite. Sample OF2378, PPL. f) Photomicrograph of
8 a type III vein, similar to that of Fig. 6e, cut by mono-mineralic type IV veins consisting of garnet
9 richer in the grossular component with respect to the previous garnet generations. Sample
10 OF2354, PPL. g) Fine-grained rodingite showing a chlorite + andradite-rich garnet vein of type
11 III cut by a brownish vesuvianite vein of type V. h) Photomicrograph of a type VI vein consisting
12 of chlorite. Sample OF2376, PPL.



1
 2 FIG. 7. Photomicrographs of fluid inclusions within rodingitic veins. a) Intragranular trails of two-
 3 phase fluid inclusions within andraditic garnet from type III vein. Sample OF2356, PPL. b)
 4 Primary fluid inclusions within vesuvianite from type V vein. Sample OF2365, PPL. c) Isolated
 5 biphasic (L + V) aqueous inclusion in vesuvianite from type V vein. Sample OF2365, PPL.

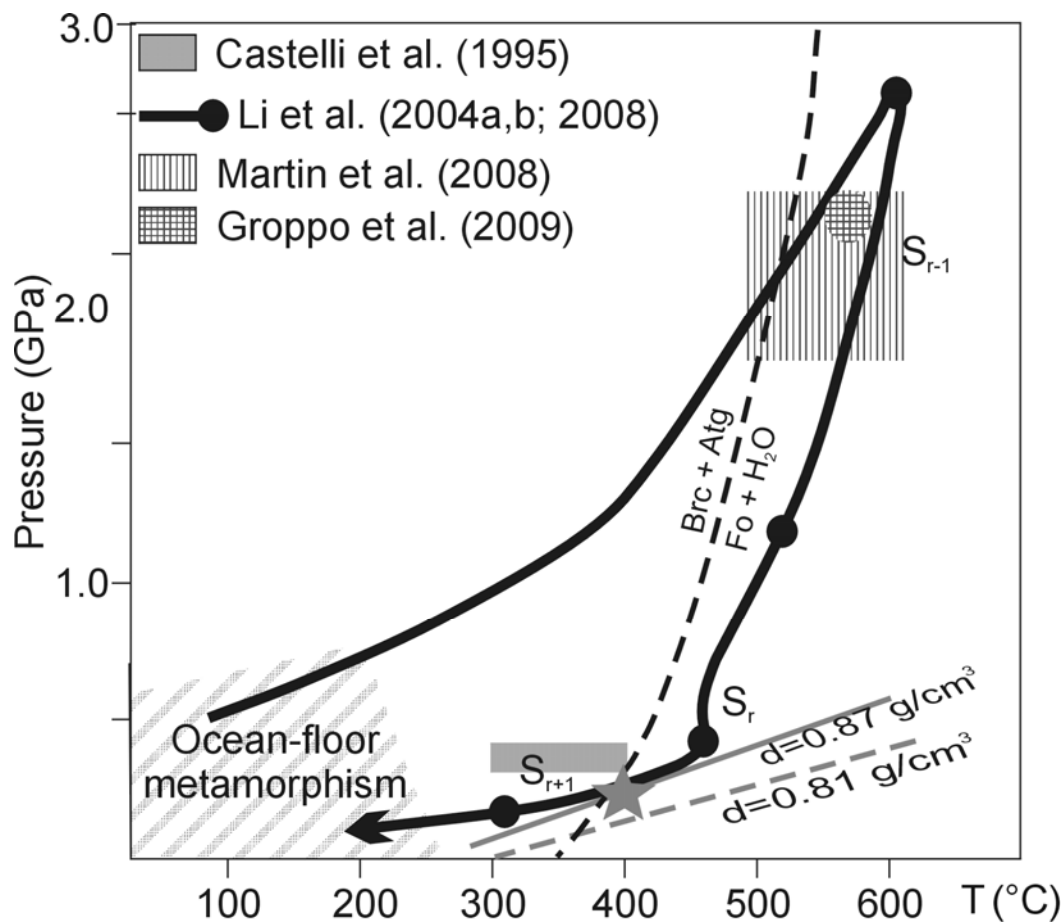


1
 2 FIG. 8. Microthermometric and Raman analyses on fluid inclusions from vesuvianite (type V
 3 veins) and andraditic garnet (type III veins). a) Histogram showing the distribution of the
 4 homogenisation temperatures (T_{hL}). The arrow indicates the maximum distribution of T_{hL} values
 5 at $T = 286.7^{\circ}C$, which has been selected for calculation of the isochores reported in Fig. 10. b)
 6 Raman spectrum, in the 4000 cm^{-1} region, of a fluid inclusion in vesuvianite indicating the
 7 presence of H_2 (peaks at 4127, 4145, 4157, and 4163 cm^{-1}) in the gas bubble.



1
 2 FIG. 9. Tectono-metamorphic evolution of the studied Bellecombe rocks. a) Rodingite and
 3 associated veins. The Grs and Adr content in the vein garnet is also reported. P = protolith. b)

- 1 Serpentinite hosting the studied rodingite. P = protolith; Kmr = Cr-chlorite ("kämmererite"). DE =
- 2 dyke emplacement. OFM = ocean-floor metamorphism.



1
 2 FIG. 10. P - T path of the Bellecombe rodingite and hosting serpentinite (modified from Li *et al.*,
 3 2008). The grey star indicates the metamorphic conditions estimated for the formation of type V
 4 vesuvianite vein. Dashed grey line: fluid isochore calculated in the H_2O - NaCl - CaCl_2 system ($d =$
 5 0.81 g/cm^3). Thick grey line: fluid isochore calculated for the same H_2O - NaCl - CaCl_2 fluid
 6 composition, after addition of 1 mole% of H_2 ($d = 0.87 \text{ g/cm}^3$). Dashed black line: Ol-out reaction
 7 curve from Li *et al.* 2004a. Dark grey box: P - T conditions estimated for the rodingitisation event
 8 in the Balangero asbestos mine (Castelli *et al.* 1995). Light grey box: P - T conditions estimated
 9 for the Atg veining in the Western Alps (Groppo & Compagnoni 2007a, 2007b). S_{r-1} : eclogite-
 10 facies foliation; S_r : main regional foliation, S_{r+1} : crenulation.

1

2 **TABLES**

Sample Analysis	OF2358 I2GT12	OF2369 grt.4	OF2369 grt.5	OF2369 I1GT8	OF2358 A2GT36	OF2358 A2GT43	OF2380 R5GT19	OF2380 R6GT22	OF2358 A3GT34
Mineral	Porph. core	Porph. rim	Neoblast	Neoblast	Type I	Type II	Type III core	Type III rim	Type IV
SiO₂	40.57	38.14	37.08	37.41	40.55	38.81	35.91	35.99	37.84
TiO₂	0.16	1.21	1.59	1.31	bdl	0.79	3.05	0.62	1.81
Cr₂O₃	bdl	bdl	0.22	7.23	bdl	0.17	0.40	0.48	bdl
Al₂O₃	21.53	18.43	11.29	9.75	21.20	14.96	4.51	6.93	13.32
Fe₂O₃	0.46	6.05	14.32	9.03	1.13	8.89	21.12	21.74	11.38
FeO	1.26	1.19	1.59	1.25	1.19	1.84	0.75	bdl	0.68
MnO	0.17	0.43	0.63	0.34	bdl	0.13	0.25	0.23	0.42
MgO	0.04	0.28	0.05	0.21	0.06	0.21	0.23	0.31	0.75
CaO	36.79	34.79	33.92	34.29	36.83	34.94	34.55	34.70	34.68
Total	100.99	100.51	100.67	100.83	100.96	100.74	100.77	100.99	100.88
Si	3.03	2.92	2.94	2.97	3.03	3.01	2.93	2.90	2.95
Ti	0.01	0.07	0.09	0.08	-	0.05	0.19	0.04	0.11
Cr	-	-	0.01	0.45	-	0.01	0.03	0.03	-
Al	1.90	1.67	1.06	0.91	1.87	1.37	0.43	0.66	1.22
Fe³⁺	0.03	0.35	0.86	0.54	0.06	0.52	1.30	1.32	0.67
Fe²⁺	0.08	0.08	0.11	0.08	0.07	0.12	0.05	-	0.04
Mn	0.01	0.03	0.04	0.02	-	0.01	0.02	0.02	0.03
Mg	0.00	0.03	0.01	0.03	0.01	0.02	0.03	0.04	0.09
Ca	2.95	2.86	2.88	2.92	2.95	2.90	3.02	3.00	2.90
Grossular	0.95	0.75	0.47	0.43	0.94	0.67	0.24	0.30	0.57
Almandine	0.03	0.03	0.04	0.03	0.03	0.04	0.02	0.00	0.01
Pyrope	0.00	0.01	0.00	0.01	0.00	0.01	0.01	0.01	0.03
Spessartine	0.00	0.01	0.01	0.01	0.00	0.00	0.01	0.01	0.01
Andradite	0.01	0.18	0.42	0.27	0.03	0.26	0.62	0.65	0.33
Uvarovite	0.00	0.00	0.01	0.22	0.00	0.01	0.01	0.02	0.00
Ti-Al Garnet	0.00	0.04	0.05	0.04	0.00	0.02	0.09	0.02	0.05


3

4 TABLE 1. Representative chemical analyses of garnets from rodingites and associated veins

5 (Type I to Type IV). bdl: below detection limit.

Sample Analysis	OF2373 V11N	OF2380 R3VES4	OF2358 I3PX5	OF2380 R4PX3	OF2369 ChI2	OF2369 ChI7
Mineral	Vesuvianite	Vesuvianite	Clinopyroxene	Clinopyroxene	Chlorite	Chlorite Type VI
SiO₂	37.09	37.40	54.96	55.30	29.41	27.39
TiO₂	3.10	0.08	bdl	0.09	-	-
Cr₂O₃	-	-	bdl	0.22	bdl	0.10
Al₂O₃	13.91	15.92	0.15	0.05	19.68	19.36
Fe₂O₃	3.34	3.93	0.81	0.07	-	-
FeO	1.29	1.51	1.56	1.15	10.75	23.25
MnO	0.04	0.28	0.14	bdl	bdl	0.28
MgO	3.29	2.53	16.99	17.50	27.12	17.36
CaO	34.83	35.41	25.25	25.44	0.10	0.09
Na₂O	-	-	0.30	0.21	0.43	0.58
H₂O	3.09	3.10	-	-	12.31	11.59
Total	100.00	100.16	100.17	100.03	99.80	100.00
Si	17.98	18.12	2.00	2.00	5.73	5.67
Ti	1.13	0.03	-	0.00	-	-
Cr	-	-	-	0.01	-	0.02
Al	7.95	9.09	0.01	0.00	4.52	4.72
Fe³⁺	1.22	1.43	0.02	0.00	-	-
Fe²⁺	0.52	0.61	0.05	0.03	1.75	4.02
Mn	0.02	0.11	0.00	0.00	-	0.05
Mg	2.38	1.83	0.92	0.95	7.88	5.35
Ca	18.09	18.38	0.98	0.99	0.00	0.02
Na	-	-	0.02	0.02	0.16	0.23
OH	10.00	10.00	-	-	16.00	16.00
Diopside			0.93	0.95		
Wollastonite			0.49	0.49		
Enstatite			0.46	0.47		
Ferrosilite			0.02	0.02		
Aegirine			0.02	0.00		
Jadeite			0.00	0.00		

1
2 TABLE 2. Representative chemical analyses of vesuvianite, clinopyroxene, and chlorite from
3 rodingites and associated veins. bdl: below detection limit.

	Vein	Mineral assemblage
earlier  later	Type I	Chl - Di - Grs garnet _(Grs 93-94)
	Type II	Adr-Grs garnet _(Adr 13-28 - Grs 60-68) + Di ± Ap
	Type III	Adr-rich garnet _(Grs 22-31 - Adr 53-69) (core) Grs-Adr garnet _(Grs 34-45 - Adr 45-65) (rim) + Chl
	Type IV	Grs-rich garnet _(Grs 50-57)
	Type V	Ves
	Type VI	Chl

1

2 TABLE 3. Relative chronology and mineral assemblages of the Bellecombe rodingitic veins

3 cross-cutting the fine-grained rodingite.

Sample	Site	Tf	Te	TmHhl	Tmice	ThL
A1	A11					291.6
A1	A12					309.7
A1	A13					304.0
A1	A14					284.8
A1	A15					295.9
A1	A16					298.4
A1	A17					265.1
A1	A18					273.9
A1	A19					267.5
A1	A101					265.4
A1	A102		-52.0	-27.5		273.9
A1	A103		-38.4	-18.3		286.9
A1	A104		-35.4	-18.3	-6.3	380.8
A1	A105		-32.5	-18.3	-6.3	375.8
A2	A21			-22.4	-5.9	270.7
A2	A22	-60.1		-24.6	-12.5	360.1
A2	A23	-58.1		-24.3	-6.1	259.7
A3	A31	-58.4		-24.2	-9.7	286.9
A3	A33	-59.7		-27.1	-10.3	292.1
A3	A34			-23.3	-13.4	263.7
A3	a35*		-52.8			279.3
A3	A36		-51.9	-18.3		284.1
A3	A310		-52.7			289.9
A3	A311	-58.1		-22.7	-11.1	294.9
A3	A312	-59.7		-20.1	-7.5	298.3
A4	A41	-58.4		-22.8		262.1
A4	A42	-58.1	-33.9	-19.6	-8.4	239.7
A4	A43	-58.4			-9.8	250.1
A5	a51*	-66.1	-52.7	-26.9	-13.9	286.7
A5	A52	-58.1	-33.6	-22.1	-9.9	282.5
A5	A53	-60.6		-28.7	-7.3	289.7
A5	A54	-64.4		-26.9	-11.2	294.1
A5	A55	-64.1		-25.5	-12.4	289.9
A5	A56	-58.2	-32.9	-19.8	-8.2	302.8
A10L	a1F*	-62.8	-42.7	-26.9	-9.2	375.1
A10L	a10L1*				-9.2	265.5
A10L	A10L3			-22.7	-7.7	265.5
A10L	A10L4	-57.4		-23.8	-8.6	271.3
A10L	a10L5*			-23.2	-8.4	271.6
A10L	a10L2*			-28.0	-8.4	261.3
A10L	A10L53			-24.7	-8.4	246.5
A10L	a10I71*			-27.8	-9.8	242.5
A10L	A10I72	-60.6	-52.1	-25.4	-12.1	248.1
A10L	a10I111*	-55.8	-47.1	-28.4	-6.9	255.4
A10L	A10L151				-13.9	286.7
A10L	A10L152	-58.0		-23.9	-10.4	246.6
A10L	A10L15			-24.3	-9.3	255.4
A10L	A10L15F			-23.9	-11.2	242.5
A10L	A4DPC1*	-63.3		-24.3	-12.9	271.1
A10L	A4DPC7*			-23.2	-7.4	283.1
A10L	A4DPC7a		-53.9	-26.2	-13.1	267.0
A10L	A4DPC7b		-53.3	-27.5	-7.4	306.0
A10L	A4DPC8*	-64.1	-42.7	-28.4	-12.9	298.2
A10L	A4DPC8b*	-58.7	-33.6	-28.0	-6.9	306.0
A10L	A4DPC8c				-9.8	298.2
A10L	A4DPC8d					279.3
A10L	A4DPC8e					271.1
A10L	A4DPC8f					271.6
A10L	A4DPC8g					375.1
A10L	A4DPC8h					265.5

1

1 TABLE 4. Representative microthermometric data of fluid inclusions from the Bellecombe
2 rodingites. Tf = freezing temperature, Te = eutectic temperature, Tm_{Hnl} = final melting
3 temperature of hydrohalite; Tm_{ice} = final melting temperature of ice; Th_L = homogenisation
4 temperature to the liquid phase. Temperatures are in °C.